Investigation of Tearing Mode Stability Near Ideal Stability Boundaries Via Asymptotic Matching Techniques

Richard Fitzpatrick [a]

Institute for Fusion Studies, Department of Physics,

University of Texas at Austin, Austin, TX 78712

[a] rfitzp@utexas.edu

I. INTRODUCTION

The calculation of the stability of a tokamak plasma to tearing perturbations is most efficiently formulated as an asymptotic matching problem in which the plasma is divided into two distinct regions.[1] In the "outer region", which comprises most of the plasma, the tearing perturbation is described by the equations of linearized, marginally-stable, ideal magnetohydrodynamics (a.k.a. the "ideal-MHD" equations). However, these equations become singular on "rational" magnetic flux-surfaces at which the perturbed magnetic field resonates with the equilibrium field. In the "inner region", which consists of a set of narrow layers centered on the various rational surfaces, non-ideal-MHD effects such as plasma inertia, resistivity, viscosity, diamagnetic flows, the ion sound radius, and perpendicular and parallel energy transport, become important.[2–5] The resistive layer solutions in the various segments of the inner region must be simultaneously asymptotically matched to the ideal-MHD solution in the outer region to produce a matrix dispersion relation that determines the growth-rates and angular rotation frequencies of the various tearing modes to which the plasma is subject.[6,7] (See Sect. A 6.)

In general, the determination of the ideal-MHD contributions to the elements of the tearing mode dispersion relation is an exceptionally challenging computational task.[8–23] One way of greatly reducing the complexity of this task is to employ an inverse aspect-ratio expanded plasma equilibrium.[24–26] In such an equilibrium, the metric elements of the flux-coordinate system can be expressed analytically in terms of a relatively small number of flux-surface functions, which represents a major simplification.[6] Another significant advantage of an inverse aspect-ratio expanded equilibrium is that the magnetic perturbation in the plasma can be efficiently matched to an exterior vacuum solution that is expressed as an expansion in toroidal functions.[10] (See Sect. C.) The aspect-ratio expansion approach to the tearing mode stability problem has been realized in the recently developed TJ code, which is described in Ref. 27.

The first aim of this paper is to document three major improvements to the TJ code.

As is well known, tearing modes in tokamak plasmas become extremely unstable as an ideal stability boundary is approached.[15,28,29] When investigating such phenomena, it is im-

perative to know the exact location of the stability boundary. Appendix B explains how the the ideal-MHD solutions in the outer region, calculated by the TJ code, can be repurposed to construct a complete set of marginally-stable ideal eigenfunctions, and how these eigenfunctions can then be used to calculate the total ideal perturbed potential energy, δW, of all possible ideal modes. Of course, the ideal stability boundary corresponds to the point at which the smallest possible value of δW passes through zero.[30,31]

Previously, the TJ code either allowed for fixed boundary calculations, or calculations in which the plasma is surrounded by a vacuum region. Appendix C describes a new capability that allows for the presence of a perfectly conducting wall in the vacuum region. The radius of the wall, relative to the plasma, can be varied.

Previously, the TJ code only calculated the "tearing stability matrix" that emanates from the ideal-MHD solution in the outer region. However, this is only half of the tearing stability problem. In order to determine the growth-rates and real frequencies of possible tearing modes, it is necessary to combine the data contained in the tearing stability matrix with data obtained from resistive layer solutions in the various segments of the inner region. Appendices D and E describe a new resistive layer model that has been implemented in the TJ code. The model takes into account plasma resistivity, plasma inertia, electron and ion diamagnetic flows, the decoupling of the electron and ion fluids on lengthscales below the ion sound radius, perpendicular momentum transport, parallel and perpendicular energy transport, and the stabilizing effect of average magnetic field-line curvature.

The second aim of the paper is to benchmark the results of the TJ toroidal tearing mode code against results from the STRIDE toroidal tearing mode code. This benchmarking exercise is described in Sect. II.

The final, and main, aim of the paper is to combine all of the new features of the TJ code in an investigation of the behavior of the growth-rates and real frequencies of tearing modes as an ideal stability boundary is approached. We are particularly interested in understanding the similarities and differences when the ideal stability boundary in question is associated with an ideal *external* kink mode and an ideal *internal* kink mode. This investigation is described in Sect. III.

Finally, the paper is summarized, and conclusions are drawn, in Sect. IV.

II. BENCHMARK OF TJ CODE AGAINST STRIDE CODE

A. Introduction

The STRIDE toroidal tearing mode code [22] is a variant of the RDCON toroidal tearing mode code.[23] Both codes are built on top of the DCON ideal stability code.[32] The three latter codes are all part of the GPEC package.[33] This section compares the tearing stability matrix, $E_{kk'}$ (see Sect. A 6), where k and k' index the various rational surfaces in the plasma, calculated by the TJ code with the equivalent symmetrized tearing stability matrix, $\hat{\Delta}_{kk'}$, calculated by the STRIDE code. (Appendix F explains how $\hat{\Delta}_{kk'}$ is related to the actual tearing stability matrix, $\Delta_{kk'}$, calculated by STRIDE.)

B. Plasma Equilibrium

In the TJ code, the plasma equilibrium is determined by the shape of the plasma boundary, which is taken to be circular in this paper, as well as two profile functions. The lowest-order safety-factor profile is written [27]

$$q(r) = \frac{q_0\,\nu\,(r/a)^2}{1-[1-(r/a)^2]^\nu}, \tag{1}$$

and the normalized (see Sect. A 1) pressure profile takes the form

$$p(r) = \frac{\beta_0}{2}\left[1-\left(\frac{r}{a}\right)^2\right]^{p_p}. \tag{2}$$

Here, r is the flux-surface label with the dimensions of length that is defined in Sect. A 2. Moreover, the magnetic axis corresponds to $r=0$, and the plasma boundary to $r=a$. Note that a is the effective inverse aspect-ratio of the plasma (given that all lengths are normalized to the major radius of the magnetic axis, R_0—see Sect. A 1.) Furthermore, $q_0 = q(0)$ is the safety-factor on the magnetic axis, and β_0 is the central plasma beta. The value of ν is adjusted to obtain the desired value of $q_a = q(a)$.

In the STRIDE code, we make use of a slightly modified form of the `lar` large-aspect-ratio, circular cross-section analytic equilibrium. This equilibrium is also characterized by

two profile functions. The normalized parallel current profile, $\sigma = \mathbf{J}\cdot\mathbf{B}/B^2$, is written

$$\sigma(r) = \frac{2}{q_0}\left[1 - \left(\frac{r}{a}\right)^2\right]^{p_\sigma}. \tag{3}$$

whereas the normalized pressure profile takes the form

$$p(r) = \frac{\beta_0}{2}\left[1 - \left(\frac{r}{a}\right)^2\right]^{p_p}. \tag{4}$$

In order to obtain (almost) the same equilibrium in the two codes (each of which is based on an expansion of the Grad-Shafranov equation in terms of the inverse aspect-ratio of the plasma), we choose the values of q_0, p_σ, β_0, and p_p, and then adjust the parameter ν in the TJ code until both codes have the same value of the safety-factor at the plasma boundary, q_a. This procedure ensures that the locations of the various rational surfaces in the plasma are almost identical in both codes. All of the TJ runs described in this paper include poloidal harmonics in the range $m = -10$ to $m = +20$.

C. Single Rational Surface

We, first, consider the stability of $n = 1$ tearing modes in a zero pressure plasma equilibrium with a circular poloidal boundary that only contain a single $n = 1$ rational surface: namely, the 2/1 surface.

1. Benchmark Test 1

The first benchmark test has plasma equilibria characterized by $q_0 = 1.1$ and $p_\sigma = 1.36$, with a range of different inverse aspect-ratios, a. Figure 1 compares the E_{11} (i.e., the tearing stability index of the 2/1 tearing mode) values calculated by the TJ code,[27] the TEAR code (which is a cylindrical tearing mode code), and the STRIDE code. It can be seen that the tearing stability indices calculated by TJ and STRIDE are in very good agreement, and that both asymptote to the stability index calculated by the TEAR code in the cylindrical limit, $a \rightarrow 0$. Given that $E_{kk'}$ is necessarily Hermitian,[27] the imaginary part of E_{11} should be zero. This is the case, to a high degree of accuracy, in both the TJ and the STRIDE codes.

2. Benchmark Test 2

The second benchmark test has plasma equilibria characterized by $q_0 = 1.1$ and $a = 0.2$, with a range of different edge safety-factor values, q_a. Figure 2 compares the E_{11} (i.e., the tearing stability index of the 2/1 tearing mode) values calculated by the TJ code, the TEAR code, and the STRIDE code. It can be seen that the tearing stability indices calculated by the TJ and STRIDE are in good agreement, except when the $q = 3$ surface very closely approaches the plasma boundary (i.e., $q_a \to 3$). Note that, according to TJ and STRIDE, E_{11} becomes very large as $q_a \to 3$ because the plasma approaches an ideal stability boundary. On the other hand, the E_{11} values calculate by TEAR shows no such increase, because the ideal stability boundary is associated with a 3/1 mode, and this mode does not couple to the 2/1 mode in a cylindrical plasma.

D. Two Rational Surfaces

Next, we consider the stability of $n = 1$ tearing modes in a plasma equilibrium with a circular poloidal boundary that contains two $n = 1$ rational surface: namely, the 2/1 surface and the 3/1 surface.

1. Benchmark Test 3

The third benchmark test has plasma equilibria characterized by $q_0 = 1.1$ and $a = 0.2$, with a range of different edge safety-factor values, q_a. Figure 3 compares the elements of the tearing stability matrix, $E_{kk'}$, calculated by the TJ and the STRIDE codes. It can be seen that the elements calculated by the two codes are in good agreement. In particular, both codes predict that $E_{21} = E_{12}$, as should be the case because $E_{kk'}$ is necessarily Hermitian.[27] Both codes also predict that the imaginary parts of E_{11} and E_{22} are zero to a high degree of accuracy (again, as should be the case, because $E_{kk'}$ is Hermitian), and the imaginary part of E_{12} and E_{21} are also zero (as should be the case, because the plasma equilibrium is up-down symmetric).

2. Benkmark Test 4

The fourth, and final, benchmark test has plasma equilibria characterized by $q_0 = 1.1$, $a = 0.2$, $p_\sigma = 2.1$, and $p_p = 2.0$, with a range of different β_0 values. Figure 4 compares the elements of the tearing stability matrix calculated by the TJ and the STRIDE codes. The TJ β_0 values have been rescaled by a factor 1.08 to compensate for the slightly different beta-limits in the slightly different TJ and STRIDE equilibria. (The STRIDE beta-limit, at which all of the elements of the $E_{kk'}$ matrix become infinite, lies at $\beta_0 = 0.025$.) Once this correction has been made, it can be seen that the elements calculated by TJ and STRIDE are in reasonably good agreement.

E. Conclusions

The elements of the tearing stability matrix calculated by the TJ and STRIDE codes are in excellent agreement with one another. Given that that the RDCON code, which is closely related to the STRIDE code, has been previously benchmarked against the MARS-F and PEST-III codes,[19,23] we can be confident that the TJ code is operating as designed.

III. TEARING MODE STABILITY NEAR IDEAL STABILITY BOUNDARIES

IV. SUMMARY AND CONCLUSION

ACKNOWLEDGEMENTS

This research was directly funded by the U.S. Department of Energy, Office of Science, Office of Fusion Energy Sciences, under contract DE-SC0021156. The author would like to thank Daniel Burgess, Nikolas Logan, J.-K. Park and J.-M. Lee for help with getting the STRIDE code to run reliably.

DATA AVAILABILITY STATEMENT

The digital data used in the figures in this paper can be obtained from the author upon reasonable request. The TJ and TEAR codes are freely available at `https://github.com/rfitzp/TJ`.

Appendix A: General Definitions

1. Normalization

Unless otherwise specified, all lengths in this paper are normalized to the major radius of the plasma magnetic axis, R_0. All magnetic field-strengths are normalized to the toroidal field-strength at the magnetic axis, B_0. All currents are normalized to $B_0\,R_0/\mu_0$. All current densities are normalized to $B_0/(\mu_0\,R_0)$. All plasma pressures are normalized to B_0^2/μ_0. All toroidal electromagnetic torques are normalized to $B_0^2\,R_0^3/\mu_0$. All energies are normalized to $B_0^2\,R_0^3/\mu_0$.

2. Coordinates

Let R, ϕ, Z be right-handed cylindrical coordinates whose Jacobian is $(\nabla R\times\nabla\phi\cdot\nabla Z)^{-1} = R$, and whose symmetry axis corresponds to the symmetry axis of the axisymmetric toroidal plasma equilibrium.

Let r, θ, ϕ be right-handed flux-coordinates whose Jacobian is

$$\mathcal{J}(r,\theta) \equiv (\nabla r\times\nabla\theta\cdot\nabla\phi)^{-1} = r\,R^2. \tag{A1}$$

Note that $r = r(R,Z)$ and $\theta = \theta(R,Z)$. The magnetic axis corresponds to $r = 0$, and the plasma-vacuum interface to $r = a$. Here, $a \ll 1$ is the effective inverse aspect-ratio of the plasma.

3. Plasma Equilibrium

Consider a tokamak plasma equilibrium whose magnetic field takes the form

$$\mathbf{B}(r,\theta) = f(r)\,\nabla\phi\times\nabla r + g(r)\,\nabla\phi = f\,\nabla(\phi - q\,\theta)\times\nabla r, \tag{A2}$$

where $q(r) = r\,g/f$ is the safety-factor. Note that $\mathbf{B}\cdot\nabla r = 0$, which implies that r is a magnetic flux-surface label. Furthermore, $B^r = 0$, $B^\theta = f/\mathcal{J}$ and $B^\phi = f\,q/\mathcal{J}$. Here, superscript/subscript denote contravariaint/covariant vector components.

Equilibrium force balance requires that $\nabla P = \mathbf{J}\times\mathbf{B}$, where $P(r)$ is the equilibrium scalar plasma pressure, and $\mathbf{J} = \nabla\times\mathbf{B}$ the equilibrium plasma current density.

4. Perturbed Magnetic Field

All perturbed quantities are assumed to vary toroidally as $\exp(-\mathrm{i}\,n\,\phi)$, where the positive integer n is the toroidal mode number of the perturbation. According to Eqs. (47), (78), (99), and (101) of Ref. 27, the radial and toroidal components of the perturbed magnetic field are written

$$\mathcal{J}\,b^r = \mathrm{i}\,\psi(r,\theta) = \sum_m \psi_m(r)\,\exp(\,\mathrm{i}\,m\,\theta), \tag{A3}$$

$$b_\phi = x(r,\theta) = n\,z(r,\theta) = n\sum_m z_m(r)\,\exp(\,\mathrm{i}\,m\,\theta), \tag{A4}$$

where

$$z_m(r) = \frac{Z_m(r) + k_m\,\psi_m(r)}{m - n\,q}. \tag{A5}$$

Here, the (not necessarily positive) integers m are poloidal mode numbers, and the sum is over all mode numbers included in the calculation. Furthermore, $k_m(r)$ is real, and is specified in Eq. (100) Ref. 27.

5. Behavior in Vicinity of Rational Surface

Suppose that there are K rational surfaces in the plasma. Let the kth surface be located at $r = r_k$, and possess the resonant poloidal mode number m_k. By definition, $m_k - n\,q(r_k) = 0$.

According to Sect. V.B of Ref. 27, the non-resonant poloidal harmonics of the solutions to the ideal-MHD equations in the outer region are continuous across the surface. On the other hand, the tearing-parity components of the resonant poloidal harmonics of the solutions behave locally as

$$\psi_{m\,k}(r_k + x) = A_{L\,k}\,|x|^{\nu_{L\,k}} + A_{S\,k}\,|x|^{\nu_{S\,k}}, \tag{A6}$$

$$Z_{m\,k}(r_k + x) = \frac{\nu_{L\,k}}{L_0}\,A_{L\,k}\,|x|^{\nu_{L\,k}} + \frac{\nu_{S\,k}}{L_0}\,A_S\,|x|^{\,\nu_{S\,k}}, \tag{A7}$$

where

$$\nu_{L\,k} = \frac{1}{2} - \sqrt{-D_{I\,k}}, \tag{A8}$$

$$\nu_{S\,k} = \frac{1}{2} + \sqrt{-D_{I\,k}}, \tag{A9}$$

$$D_{I\,k} = -\left[\frac{2\,(1-q^2)}{s^2}\,r\,\frac{dP}{dr}\right]_{r_k} - \frac{1}{4}, \tag{A10}$$

$$L_0 = -\left(\frac{L_{m_k}^{m_k}}{m_k\,s}\right)_{r_k}, \tag{A11}$$

$$L_{m_k}^{m_k}(r) = m_k^2\,c_{m_k}^{m_k}(r) + n^2\,r^2, \tag{A12}$$

$$c_{m_k}^{m_k}(r) = \oint |\nabla r|^{-2}\,\frac{d\theta}{2\pi}, \tag{A13}$$

and $s(r) = d\ln q/d\ln r$. Here, the tearing-parity component is such that $\psi_{m_k}(r_k - x) = \psi_{m_k}(r_k + x)$ and $Z_{m_k}(r_k - x) = Z_{m_k}(r_k + x)$. Moreover, $A_{L\,k}$ is termed the coefficient of the "large" solution, whereas $A_{S\,k}$ is the coefficient of the "small" solution. Furthermore, $D_{I\,k}$ is the ideal Mercier interchange parameter (which needs to be negative to ensure stability to localized interchange modes),[34–36] and $\nu_{L\,k}$ and $\nu_{S\,k}$ are termed the Mercier indices.

It is helpful to define the quantities [27]

$$\Psi_k = r_k^{\nu_{L\,k}}\left(\frac{\nu_{S\,k} - \nu_{L\,k}}{L_{m_k}^{m_k}}\right)_{r_k}^{1/2} A_{L\,k}, \tag{A14}$$

$$\Delta\Psi_k = r_k^{\nu_{S\,k}}\left(\frac{\nu_{S\,k} - \nu_{L\,k}}{L_{m_k}^{m_k}}\right)_{r_k}^{1/2} 2\,A_{S\,k}, \tag{A15}$$

at each rational surface in the plasma. Here, the complex parameter Ψ_k is a measure of the reconnected helical magnetic flux at the kth rational surface, whereas the complex parameter

$\Delta\Psi_k$ is a measure of the strength of a localized current sheet that flows parallel to the equilibrium magnetic field at the surface. The net toroidal electromagnetic torque acting on the plasma is [27]

$$T_\phi = 2\pi^2\, n \sum_{k=1,K} \mathrm{Im}(\Psi_k^*\, \Delta\Psi_k). \tag{A16}$$

6. Tearing Mode Dispersion Relation

According to Sect. VIII.D of Ref. 27, the tearing mode dispersion relation takes the form

$$\sum_{k'=1,K} (E_{kk'} - \Delta_k\, \delta_{kk'})\, \Psi_{k'} = 0 \tag{A17}$$

for $k = 1, K$, where $E_{kk'}$ is an Hermitian matrix determined from the solution of the ideal-MHD equations in the outer region, and $\Delta_k \equiv \Delta\Psi_k/\Psi_k$ is a complex quantity that characterizes the tearing-parity response of the resistive layer at the kth rational surface to the outer solution. In general, Δ_k is a function of the growth-rate and phase-velocity of the reconnected helical magnetic flux at the surface.

Appendix B: Calculation of Ideal Stability

1. Plasma Perturbation

The perturbed magnetic field associated with an ideal perturbation is written [30,31]

$$\mathbf{b} = \nabla \times (\boldsymbol{\xi} \times \mathbf{B}), \tag{B1}$$

where $\boldsymbol{\xi}$ is the plasma displacement. According to Eqs. (2), (25), (26), and (101) of Ref. 27,

$$\mathcal{J}\, b^r = \left(\frac{\partial}{\partial\theta} - \mathrm{i}\, n\, q\right) y = \mathrm{i}\, \psi(r,\theta), \tag{B2}$$

where

$$y(r,\theta) = f\, \xi^r. \tag{B3}$$

Furthermore, Eqs. (38), (39), (48), and (78) of Ref. 27 yield

$$b_\theta = -\frac{\alpha_g}{\mathrm{i}\, n}\left(\frac{\partial}{\partial\theta} - \mathrm{i}\, n\, q\right) y + \alpha_p\, R^2\, y + \mathrm{i}\,\frac{\partial z}{\partial\theta}, \tag{B4}$$

where

$$\alpha_p(r) = \frac{r\, dP/dr}{f^2}, \tag{B5}$$

$$\alpha_g(r) = \frac{dg/dr}{f}. \tag{B6}$$

Thus,

$$\mathbf{B}\cdot\mathbf{b} - \xi^r\,\frac{dP}{dr} = B^\theta\, b_\theta + B^\phi\, b_\phi - \xi^r\,\frac{dP}{dr} = \frac{\mathrm{i}\, f}{\mathcal{J}}\left(\frac{\partial}{\partial\theta} - \mathrm{i}\, n\, q\right)\left(\frac{\alpha_g}{n}\, y + z\right). \tag{B7}$$

2. Plasma Potential Energy

The perturbed ideal-MHD force operator in the plasma takes the well-known form [30,31]

$$\mathbf{F}(\boldsymbol{\xi}) = \nabla(\Gamma\, P\,\nabla\cdot\boldsymbol{\xi}) - \mathbf{B}\times(\nabla\times\mathbf{b}) + \nabla(\boldsymbol{\xi}\cdot\nabla P) + \mathbf{J}\times\mathbf{b}, \tag{B8}$$

where $\Gamma = 5/3$ is the plasma ratio of specific heats. The perturbed plasma potential energy in the region lying between the magnetic flux-surfaces whose labels are r_1 and r_2 can be written [31]

$$\delta W_{12} = \frac{1}{2}\int_{r_1}^{r_2}\oint\oint [\Gamma\, P\,(\nabla\cdot\boldsymbol{\xi}^*)\,(\nabla\cdot\boldsymbol{\xi}) + \nabla\times(\boldsymbol{\xi}^*\times\mathbf{B})\cdot\mathbf{b} + (\nabla\cdot\boldsymbol{\xi}^*)\,(\boldsymbol{\xi}\cdot\nabla P)$$
$$+\mathbf{J}\times\boldsymbol{\xi}^*\cdot\mathbf{b}]\,\mathcal{J}\,dr\,d\theta\,d\phi. \tag{B9}$$

Now,

$$\Gamma\, P\,(\nabla\cdot\boldsymbol{\xi}^*)\,(\nabla\cdot\boldsymbol{\xi}) = \nabla\cdot(\Gamma\, P\,\boldsymbol{\xi}^*\,\nabla\cdot\boldsymbol{\xi}) - \boldsymbol{\xi}^*\cdot\nabla(\Gamma\, P\,\nabla\cdot\boldsymbol{\xi}), \tag{B10}$$

$$\nabla\times(\boldsymbol{\xi}^*\times\mathbf{B})\cdot\mathbf{b} = \nabla\cdot[(\boldsymbol{\xi}^*\times\mathbf{B})\times\mathbf{b}] + \boldsymbol{\xi}^*\times\mathbf{B}\cdot\nabla\times\mathbf{b}, \tag{B11}$$

$$(\nabla\cdot\boldsymbol{\xi}^*)\,(\boldsymbol{\xi}\cdot\nabla P) = \nabla\cdot(\boldsymbol{\xi}^*\,\boldsymbol{\xi}\cdot\nabla P) - \boldsymbol{\xi}^*\cdot\nabla(\boldsymbol{\xi}\cdot\nabla P), \tag{B12}$$

so

$$\delta W_{12} = \frac{1}{2}\int_{r_1}^{r_2}\oint\oint \{\nabla\cdot[\Gamma\, P\,\boldsymbol{\xi}^*\,\nabla\cdot\boldsymbol{\xi} + (\boldsymbol{\xi}^*\times\mathbf{B})\times\mathbf{b} + \boldsymbol{\xi}^*\,\boldsymbol{\xi}\cdot\nabla P]$$

$$-\boldsymbol{\xi}^* \cdot [\nabla(\Gamma\, P\, \nabla\cdot\boldsymbol{\xi}) - \mathbf{B}\times(\nabla\times\mathbf{b}) + \nabla(\boldsymbol{\xi}\cdot\nabla P) + \mathbf{J}\times\mathbf{b}]\}\, \mathcal{J}\, dr\, d\theta\, d\phi, \tag{B13}$$

which yields

$$\delta W_{12} = \frac{1}{2}\left(\oint\oint \mathcal{J}\, \nabla r\cdot[\Gamma\, P\, \boldsymbol{\xi}^*\, \nabla\cdot\boldsymbol{\xi} + (\boldsymbol{\xi}^*\times\mathbf{B})\times\mathbf{b} + \boldsymbol{\xi}^*\,\boldsymbol{\xi}\cdot\nabla P]\, d\theta\, d\phi\right)_{r_1}^{r_2}$$
$$-\frac{1}{2}\int_{r_1}^{r_2}\oint\oint \boldsymbol{\xi}^*\cdot\mathbf{F}(\boldsymbol{\xi})\, \mathcal{J}\, dr\, d\theta\, d\phi, \tag{B14}$$

or

$$\delta W_{12} = \frac{1}{2}\left[\oint\oint \mathcal{J}\, \xi^{r\,*}\left(\Gamma\, P\, \nabla\cdot\boldsymbol{\xi} - \mathbf{B}\cdot\mathbf{b} + \xi^r\,\frac{dP}{dr}\right) d\theta\, d\phi\right]_{r_1}^{r_2}$$
$$-\frac{1}{2}\int_{r_1}^{r_2}\oint\oint \boldsymbol{\xi}^*\cdot\mathbf{F}(\boldsymbol{\xi})\, \mathcal{J}\, dr\, d\theta\, d\phi, \tag{B15}$$

where use has been made of the fact that $\mathbf{B}\cdot\nabla r = 0$. However, in the TJ code, the marginally-stable ideal-MHD plasma perturbation in the outer region is calculated assuming that $\mathbf{F}(\boldsymbol{\xi}) = \mathbf{0}$ and $\nabla\cdot\boldsymbol{\xi} = 0$.[27] Thus, making use of Eqs. (B3) and (B7), we obtain

$$\delta W_{12} = \frac{1}{2}\int_{r_1}^{r_2}\left[-\mathrm{i}\, y^*\left(\frac{\partial}{\partial\theta} - \mathrm{i}\, n\, q\right)\left(\frac{\alpha_g}{n}\, y + z\right) d\theta\, d\phi\right]_{r_1}^{r_2}, \tag{B16}$$

which reduces to

$$\delta W_{12} = \pi^2\left[\sum_m y_m^*\,(m - n\, q)\left(\frac{\alpha_g}{n}\, y_m + z_m\right)\right]_{r_1}^{r_2}, \tag{B17}$$

where $y(r,\theta) = \sum_m y_m(r)\, \exp(\,\mathrm{i}\, m\,\theta)$.

Now, according to Eq. (98) of Ref. 27,

$$y_m(r) = \left(\frac{\psi_m}{m - n\, q}\right)_r. \tag{B18}$$

Thus, we get

$$\delta W_{12} = \pi^2\left(\sum_m \psi_m^*\, \chi_m\right)_{r_1}^{r_2} \tag{B19}$$

where

$$\chi_m(r) = \left(\frac{\tilde{k}_m\, \psi_m + Z_m}{m - n\, q}\right)_r, \tag{B20}$$

$$\tilde{k}_m(r) = \left(k_m + \frac{\alpha_g}{n}\right)_r = \left[\frac{\alpha_g\,(m\, q\, c_m^m + n\, r^2) + \alpha_p\, m\, d_m^m}{m^2\, c_m^m + n^2\, r^2}\right]_r, \tag{B21}$$

and use has been made of Eq. (100) Ref. 27. Here, $\tilde{k}_m(r)$ is real, and

$$d_m^m(r) = \oint |\nabla r|^{-2}\, R^2\, \frac{d\theta}{2\pi}. \tag{B22}$$

3. Magnetic Axis

Let the $\psi_m(r)$ and the $\chi_m(r)$ be solutions of the ideal-MHD equations in the outer region that are well behaved at $r = 0$. Such solutions vary as $r^{|m|}$. (For the special case $m = 0$, $\chi_0 \sim 1$ and $\psi_0 = 0$.) It follows that [27]

$$\left(\sum_m \psi_m^*\, \chi_m\right)_0 = 0. \tag{B23}$$

Hence,

$$\delta W_p(r) = \pi^2 \left(\sum_m \psi_m^*\, \chi_m\right)_r \tag{B24}$$

is the perturbed plasma potential energy in the region lying between the magnetic axis and the magnetic flux-surface whose label is r.

4. Rational Surfaces

At the kth rational surface, $r = r_k$, the non-resonant components of ψ_m and χ_m are continuous, the large solution is absent (i.e., $\Psi_k = 0$), but the small solution is present (i.e., $\Delta\Psi_k = 0$). (See Sect. A 5.) It is easily shown that $\sum_m \psi_m^*\, \chi_m$ remains finite at $r = r_k$ (which would not be the case if $\Psi_k \neq 0$), and [27]

$$\left(\sum_m \psi_m^*\, \chi_m\right)_{r_{k-}}^{r_{k+}} = 0. \tag{B25}$$

In other words, there is no contribution to the perturbed potential energy from the surface. Thus, Eq. (B24) holds even when the region between the magnetic axis and the flux-surface whose label is r contains rational surfaces. Thus, the total plasma potential energy is

$$\delta W_p = \pi^2 \left(\sum_m \psi_m^*\, \chi_m\right)_{a_-}, \tag{B26}$$

where $r = a_-$ corresponds to an equilibrium magnetic flux that lies just inside the plasma-vacuum interface.

5. Toroidal Electromagnetic Torque

The flux-surface averaged toroidal electromagnetic torque acting on the plasma is [27,31]

$$T_\phi = \mathrm{i}\, n\, \pi^2 \left(\sum_m \frac{Z_m^*\, \psi_m - \psi_m^*\, Z_m}{m - n\, q} \right)_{a-} = \mathrm{i}\, n\, \pi^2 \left(\sum_m \chi_m^*\, \psi_m - \psi_m^*\, \chi_m \right)_{a-}$$
$$= 2\, n\, \mathrm{Im}(\delta W_p), \tag{B27}$$

where use has been made of Eqs. (B20) and (B24). However, according to Eq. (A16), this torque must be zero for ideal solutions, which are characterized by $\Psi_k = 0$ (i.e., zero reconnected magnetic flux at the various rational surfaces in the plasma).[27] It follows that the total plasma potential energy, δW_p, is necessarily a real quantity.

6. Marginally-Stable Ideal Eigenfunctions

We can construct a complete set of marginally-stable ideal eigenfuctions in the outer region from the ideal-MHD solutions in the outer region calculated by the TJ code as follows:

$$\psi^i_{m\,m'}(r) = \psi^a_{m\,m'}(r) - \sum_{k=1,K} \psi^u_{m\,k}(r)\, \Pi^a_{k\,m'}, \tag{B28}$$

$$Z^i_{m\,m'}(r) = Z^a_{m\,m'}(r) - \sum_{k=1,K} Z^u_{m\,k}(r)\, \Pi^a_{k\,m'}. \tag{B29}$$

Here, m labels the poloidal harmonic of the solution, m' labels the solution itself, and k labels the various rational surfaces in the plasma. There are as many solutions as there are poloidal harmonics included in the calculation. All other quantities are defined in Sects. VIII.B–VIII.D of Ref. 27. It follows from the definitions of the various quantities in the previous two equations that the reconnected magnetic fluxes at the rational surfaces in the plasma associated with the ideal eigenfunctions are all zero (i.e., $\Psi_k = 0$ for all k). We can also write

$$\chi^i_{m\,m'}(r) = \left(\frac{\tilde{k}_m\, \psi^i_{m\,m'} + Z^i_{m\,m'}}{m - n\, q} \right)_r, \tag{B30}$$

where use has been made of Eq. (B20).

7. Plasma Energy Matrix

We can write a general ideal solution just inside the plasma-vacuum interface as

$$\psi_m(a) = \sum_{m'} \psi^i_{m\,m'}(a)\,\alpha_{m'}, \tag{B31}$$

$$\chi_m(a_-) = \sum_{m'} \chi^i_{m\,m'}(a_-)\,\alpha_{m'}, \tag{B32}$$

where the α_m are arbitrary complex coefficients. Note that the $\psi_m(r)$ are continuous across the plasma-vacuum interface, whereas the $\chi_m(r)$ are generally discontinuous. The previous two equations can be written more succinctly as

$$\underline{\psi} = \underline{\underline{\psi}}_i\,\underline{\alpha}, \tag{B33}$$

$$\underline{\chi} = \underline{\underline{\chi}}_i\,\underline{\alpha}, \tag{B34}$$

where $\underline{\psi}$ is the column vector of the $\psi_m(a)$ values, $\underline{\chi}$ is the column vector of the $\chi_m(a_-)$ values, $\underline{\underline{\psi}}_i$ is the matrix of the $\psi^i_{mm'}(a)$ values, $\underline{\underline{\chi}}_i$ is the matrix of the $\chi^i_{mm'}(a_-)$ values, and $\underline{\alpha}$ the column vector of the α_m values. Equation (B26) then becomes

$$\delta W_p = \pi^2\,\underline{\psi}^\dagger\,\underline{\chi}, \tag{B35}$$

or

$$\delta W_p = \pi^2\,\underline{\alpha}^\dagger\,\underline{\underline{\psi}}^\dagger_i\,\underline{\underline{\chi}}_i\,\underline{\alpha}. \tag{B36}$$

The fact that δW_p is real implies that

$$\underline{\underline{\psi}}^\dagger_i\,\underline{\underline{\chi}}_i = \underline{\underline{\chi}}^\dagger_i\,\underline{\underline{\psi}}_i. \tag{B37}$$

Let us define the "plasma energy matrix", $\underline{\underline{W}}_p$, such that

$$\underline{\underline{\chi}}_i = \underline{\underline{W}}_p\,\underline{\underline{\psi}}_i. \tag{B38}$$

It is easily seen that

$$\underline{\underline{\psi}}^\dagger_i\,\underline{\underline{\chi}}_i = \underline{\underline{\psi}}^\dagger_i\,\underline{\underline{W}}_p\,\underline{\underline{\psi}}_i, \tag{B39}$$

$$\underline{\underline{\chi}}_i^{\dagger}\,\underline{\underline{\psi}}_i = \underline{\underline{\psi}}_i^{\dagger}\,\underline{\underline{W}}_p^{\dagger}\,\underline{\underline{\psi}}_i. \tag{B40}$$

Making use of Eq. (B37), we obtain

$$\underline{\underline{\psi}}_i^{\dagger}\,\underline{\underline{W}}_p\,\underline{\underline{\psi}}_i = \underline{\underline{\psi}}_i^{\dagger}\,\underline{\underline{W}}_p^{\dagger}\,\underline{\underline{\psi}}_i, \tag{B41}$$

which implies that $\underline{\underline{W}}_p$ is an Hermitian matrix.

8. Total Potential Energy

The total perturbed potential energy of the plasma-vacuum system can be written [30,31]

$$\delta W = \delta W_p + \delta W_v, \tag{B42}$$

where

$$\delta W_v = \frac{1}{2}\int_{a+}^{\infty}\oint\oint \mathbf{b}^*\cdot\mathbf{b}\,\mathcal{J}\,dr\,d\theta\,d\phi \tag{B43}$$

is the perturbed potential energy of the surrounding vacuum.[30,31] Here, $r = a_+$ corresponds to an equilibrium magnetic flux-surface that lies just outside the plasma-vacuum interface.

9. Vacuum Potential Energy

In the vacuum region, we can write the curl- and divergence-free perturbed magnetic field in the form $\mathbf{b} = \mathrm{i}\,\nabla V$, where $\nabla^2 V = 0$. Hence, the vacuum potential energy is

$$\begin{aligned}\delta W_v &= \frac{1}{2}\int_{a+}^{\infty}\oint\oint \nabla V\cdot\nabla V^*\,\mathcal{J}\,dr\,d\theta\,d\phi\\ &= \frac{1}{2}\int_{a+}^{\infty}\oint\oint \nabla\cdot(V\,\nabla V^*)\,\mathcal{J}\,dr\,d\theta\,d\phi = -\frac{1}{2}\left(\oint\oint \mathcal{J}\,\nabla r\cdot\nabla V^*\,V\,d\theta\,d\phi\right)_{a_+},\end{aligned} \tag{B44}$$

assuming that $V(r,\theta)\to 0$ as $r\to\infty$ if there is no wall surrounding the plasma, or $\nabla V\cdot d\mathbf{S} = 0$ if a perfectly-conducting wall surrounds the plasma. But, Eq. (210) of Ref. 27 implies that

$$\mathcal{J}\,\nabla V\cdot\nabla r = \psi, \tag{B45}$$

so we deduce that

$$\delta W_v = -\frac{1}{2}\left(\oint\oint \psi^*\,V\,d\theta\,d\phi\right)_{a_+} = -\pi^2\left(\sum_m \psi_m^*\,V_m\right)_{a_+}, \tag{B46}$$

where $V(r,\theta) = \sum_m V_m(r)\,\exp(\,\mathrm{i}\,m\,\theta)$. However, making use of Eq. (214) of Ref. 27, we get

$$\delta W_v = -\pi^2 \left(\sum_m \psi_m^*\,\chi_m \right)_{a_+}, \tag{B47}$$

where

$$\chi_m = \frac{Z_m}{m - n\,q}. \tag{B48}$$

Note that the previous equation is consistent with Eq. (B20) because, according to Eq. (B21), $\tilde{k}_m = 0$ in the vacuum region, given that $\alpha_g = \alpha_p = 0$ in the vacuum.

Combining Eqs. (B26), (B42), and (B47), we deduce that

$$\delta W = \pi^2 \left(\sum_m \psi_m^*\,J_m \right)_{\epsilon}, \tag{B49}$$

where

$$J_m = -\,[\chi_m]_{a_-}^{a_+}\,. \tag{B50}$$

10. Boundary Current Sheet

Now, $\alpha_p = \alpha_g = 0$ at the plasma-vacuum interface, assuming that the equilibrium current is zero there, which implies that $k_m = \tilde{k}_m = 0$ at the interface, where use has been made of Eq. (B21), as well as Eq. (100) of Ref. 27. It follows from Eqs. (78) and (99) of Ref. 27, combined with Eq. (B48), that

$$x_m = n\,\chi_m \tag{B51}$$

at the plasma-vacuum interface, where $x(r,\theta) = \sum_m x_m(r)\,\exp(\,\mathrm{i}\,m\,\theta)$. Suppose that there is a perturbed current sheet on the interface. Thus, if $\mathbf{K}$ is the current sheet density then Eqs. (66) and (67) of Ref. 27 suggest that

$$\mathcal{J}\,K_m^\theta = n\,J_m, \tag{B52}$$

$$\mathcal{J}\,K_m^\phi = m\,J_m, \tag{B53}$$

where use has been made of Eqs. (B50) and (B51). Let us write

$$\mathbf{K} = \mathrm{i}\,\nabla J \times \nabla r, \tag{B54}$$

where $J(\theta,\phi) = J(\theta)\,\exp(-\mathrm{i}\,n\,\phi)$, which ensures that $\nabla\cdot\mathbf{K} = 0$. It follows from (A8) and (A9) of Ref. 27 that

$$\mathcal{J}\,K^\theta = \mathrm{i}\,\frac{\partial J}{\partial\phi}, \tag{B55}$$

$$\mathcal{J}\,K^\phi = -\mathrm{i}\,\frac{\partial J}{\partial\theta}. \tag{B56}$$

Hence, if we expand the previous two equations as Fourier series in θ then we reproduce Eqs. (B52) and (B53), which implies that the J_m defined in Eq. (B50) are the Fourier components of the $J(\theta)$ function introduced in Eq. (B54).

As described in Ref. 31, the marginally-stable ideal eigenfunctions feature a perturbed current sheet on the vacuum-plasma interface because they do not satisfy the perturbed pressure-balance boundary condition. However, these current sheets are entirely fictitious. The true ideal eigenfunctions (which, unlike the marginally-stable ideal eigenfunctions, take plasma inertia into account) satisfy the pressure-balance boundary condition (and, therefore, have no associated current sheets). Current sheets are permitted because the marginally-stable ideal eigenfunctions are "trial solutions" used to determine ideal stability, rather than actual physical solutions.

11. Determination of Ideal Stability

According to Eq. (215) of Ref. 27, combined with Eq. (B48),

$$\chi_m(a_+) = \sum_{m'} H_{m\,m'}\,\psi_{m'}(a), \tag{B57}$$

where the "vacuum matrix", $H_{mm'}$, is Hermitian. (See Sect. VI.G of Ref. 27.) Hence, it follows from Eq. (B50) that

$$J_m = \chi_m(a_-) - \sum_{m'} H_{m\,m'}\,\psi_m(a). \tag{B58}$$

Making use of Eq. (B49), we can write

$$\delta W = \pi^2\,\underline{\psi}^\dagger\,\underline{J}, \tag{B59}$$

where

$$\underline{J} = \underline{\chi} + \underline{\underline{W}}_v \, \underline{\psi}. \tag{B60}$$

Here, $\underline{J}$ is the column vector of the J_m values, and the "vacuum energy matrix", $\underline{\underline{W}}_v$, is the Hermitian matrix of the $-H_{m\,m'}$ values. Making use of Eqs. (B33), (B34), and (B38), we get

$$\underline{J} = \underline{\underline{W}} \, \underline{\psi}, \tag{B61}$$

and

$$\delta W = \underline{\alpha}^\dagger \, \underline{\underline{\psi}}_i^\dagger \, (\underline{\chi}_i + \underline{\underline{W}}_v \, \underline{\underline{\psi}}_i) \, \underline{\alpha} = \underline{\alpha}^\dagger \, \underline{\underline{\psi}}_i^\dagger \, \underline{\underline{W}} \, \underline{\underline{\psi}}_i \, \underline{\alpha}, \tag{B62}$$

where

$$\underline{\underline{W}} = \underline{\underline{W}}_p + \underline{\underline{W}}_v. \tag{B63}$$

Note that $\underline{\underline{W}}_p$ and $\underline{\underline{W}}_v$ are both Hermitian, so $\underline{\underline{W}}$ is also Hermitian. Thus the "total energy matrix", $\underline{\underline{W}}$, possesses real eigenvalues and orthonormal eigenvectors, $\underline{\beta}_m$. Let $(\underline{\beta}_{m'})_m = \beta_{m\,m'}$, and let $\underline{\underline{\beta}}$ be the matrix of the $\beta_{mm'}$ values. It follows that $\underline{\underline{\beta}}^\dagger \, \underline{\underline{\beta}} = \underline{\underline{1}}$. We conclude that there are as many linearly independent ideal eigenmodes of the plasma as there are poloidal harmonics included in the calculation. The mth eigenmode has the associated energy

$$\delta W_m = \delta W_{p\,m} + \delta W_{v\,m}, \tag{B64}$$

where

$$\delta W_m = \underline{\beta}_m^\dagger \, \underline{\underline{W}} \, \underline{\beta}_m, \tag{B65}$$

$$\delta W_{p\,m} = \underline{\beta}_m^\dagger \, \underline{\underline{W}}_p \, \underline{\beta}_m, \tag{B66}$$

$$\delta W_{v\,m} = \underline{\beta}_m^\dagger \, \underline{\underline{W}}_v \, \underline{\beta}_m. \tag{B67}$$

Note that δW_m, $\delta W_{p\,m}$ and $\delta W_{v\,m}$ are all real quantities. Moreover, $\delta W_{p\,m}$ and $\delta W_{v\,m}$ can be interpreted as the plasma and vacuum contributions to δW_m, respectively. Finally,

$$\delta W = \sum_m |\hat{\alpha}_m|^2 \, \delta W_m, \tag{B68}$$

where $\hat{\underline{\alpha}} = \underline{\underline{\beta}}^\dagger \, \underline{\underline{\psi}}_i \, \underline{\alpha}$. As is well known, the plasma is ideally unstable if $\delta W < 0$ for any possible ideal peturbation.[30,31] Thus, given that the $\hat{\alpha}_m$ are arbitrary, we deduce that if any of the δW_m are negative then the plasma is ideally unstable.

Appendix C: Vacuum Solution

1. Toroidal Coordinates

Let μ, η, ϕ be right-handed toroidal coordinates defined such that

$$R = \frac{\sinh\mu}{\cosh\mu - \cos\eta}, \tag{C1}$$

$$Z = \frac{\sin\eta}{\cosh\mu - \cos\eta}. \tag{C2}$$

The scale-factors of the toroidal coordinate system are

$$h_\mu = h_\eta = \frac{1}{\cosh\mu - \cos\eta} \equiv h, \tag{C3}$$

$$h_\phi = \frac{\sinh\mu}{\cosh\mu - \cos\eta} = h\,\sinh\mu. \tag{C4}$$

Moreover,

$$\mathcal{J}' \equiv (\nabla\mu \times \nabla\eta \cdot \nabla\phi) = h^3\,\sinh\mu. \tag{C5}$$

2. Perturbed Magnetic Field

The curl-free perturbed magnetic field in the vacuum region is written $\mathbf{b} = \mathrm{i}\,\nabla V$, where $\nabla^2 V = 0$. The most general solution to Laplace's equation is

$$V(z,\eta) = \sum_m (z - \cos\eta)^{1/2}\,U_m(z)\,\mathrm{e}^{-\mathrm{i}\,m\,\eta}, \tag{C6}$$

$$U_m(z) = p_m\,\hat{P}^n_{|m|-1/2}(z) + q_m\,\hat{Q}^n_{m-1/2}(z), \tag{C7}$$

where $z = \cosh\mu$, the p_m and q_m are arbitrary complex coefficients, and

$$\hat{P}^n_{|m|-1/2}(z) = \cos(|m|\,\pi)\,\frac{\sqrt{\pi}\,\Gamma(|m| + 1/2 - n)\,a^{\,|m|}}{2^{\,|m|-1/2}\,|m|!}\,P^n_{|m|-1/2}(z), \tag{C8}$$

$$\hat{Q}^n_{|m|-1/2}(z) = \cos(n\,\pi)\,\cos(|m|\,\pi)\,\frac{2^{\,|m|-1/2}\,|m|!}{\sqrt{\pi}\,\Gamma(|m| + 1/2 + n)\,a^{\,|m|}}\,Q^n_{|m|-1/2}(z). \tag{C9}$$

Here, the $P^n_{m-1/2}(z)$ and $Q^n_{|m|-1/2}(z)$ are toroidal functions,[37] and $\Gamma(z)$ is a gamma function.[38]

3. Toroidal Electromagnetic Angular Momentum Flux

The outward flux of toroidal angular momentum across a constant-z surface is

$$T_\phi(z) = -\oint\oint \mathcal{J}'\, b_\phi\, b^\mu\, d\eta\, d\phi \tag{C10}$$

$$= \mathrm{i}\, n\, \pi^2 \sum_m (p_m\, q_m^* - q_m\, p_m^*)\, (z^2-1)\, \mathcal{W}(\hat{P}^n_{|m|-1/2}, \hat{Q}^n_{|m|-1/2}), \tag{C11}$$

where $\mathcal{W}(f,g) \equiv f\, dg/dz - g\, df/dz$. But,[39]

$$\mathcal{W}(\hat{P}^n_{|m|-1/2}, \hat{Q}^n_{|m|-1/2}) = \cos(n\,\pi)\, \frac{\Gamma(|m|+1/2-n)}{\Gamma(|m|+1/2+n)}\, \mathcal{W}(P^n_{|m|-1/2}, Q^n_{|m|-1/2})$$

$$= \frac{1}{1-z^2}, \tag{C12}$$

where use has been made of Eqs. (C8) and (C9), so

$$T_\phi(z) = 2\pi^2\, n \sum_m \mathrm{Im}(q_m^*\, p_m). \tag{C13}$$

Note that T_ϕ is independent of z, as must be the case because there are no angular momentum sources in the vacuum region.

4. Solution in Vacuum Region

In the large-aspect ratio limit, $r \ll 1$, it can be demonstrated that [39]

$$z \simeq \frac{1}{r}, \tag{C14}$$

$$z^{\,1/2}\, \hat{P}^{\,n}_{-1/2}(z) \simeq \frac{1}{2} \ln\left(\frac{8\,z}{\zeta_n}\right), \tag{C15}$$

$$z^{1/2}\, \hat{P}^n_{|m|-1/2}(z) \simeq \frac{\cos(|m|\,\pi)\, (a\,z)^{|m|}}{|m|}, \tag{C16}$$

$$z^{1/2}\, \hat{Q}^n_{|m|-1/2}(z) \simeq \frac{\cos(|m|\,\pi)\, (a\,z)^{-|m|}}{2}, \tag{C17}$$

$$\zeta_n = \exp\left(\sum_{j=1,n} \frac{2}{2\,j-1}\right). \tag{C18}$$

Note that Eq. (C16) only applies to $|m| > 0$.

The plasma-vacuum interface lies at $r = a$. Suppose that the plasma is surrounded by a perfectly conducting wall at $r = b_w\, a$, where $b_w \geq 1$. In the vacuum region, $a \leq r \leq b_w\, a$, lying between the plasma and the wall, we can write

$$\underline{V}(r) = \underline{\underline{\mathcal{P}}}(r)\,\underline{p} + \underline{\underline{\mathcal{Q}}}(r)\,\underline{q}, \tag{C19}$$

$$\underline{\psi}(r) = \underline{\underline{\mathcal{R}}}(r)\,\underline{p} + \underline{\underline{\mathcal{S}}}(r)\,\underline{q}, \tag{C20}$$

where $\underline{V}(r)$ is the vector of the $V_m(r)$ values (see Sect. B 9), $\underline{\psi}(r)$ is the vector of the $\psi_m(r)$ values [see Eq. (A3)], $\underline{\underline{\mathcal{P}}}(r)$ is the matrix of the

$$\mathcal{P}_{mm'}(r) = \oint_r (z - \cos\eta)^{1/2}\, \hat{P}^n_{|m'|-1/2}(z)\, \exp[-\mathrm{i}\,(m\,\theta + m'\,\eta)]\, \frac{d\theta}{2\pi} \tag{C21}$$

values, $\underline{\underline{\mathcal{Q}}}(r)$ is the matrix of the

$$\mathcal{Q}_{mm'}(r) = \oint_r (z - \cos\eta)^{1/2}\, \hat{Q}^n_{|m'|-1/2}(z)\, \exp[-\mathrm{i}\,(m\,\theta + m'\,\eta)]\, \frac{d\theta}{2\pi} \tag{C22}$$

values, $\underline{\underline{\mathcal{R}}}(r)$ is the matrix of the

$$\begin{aligned}\mathcal{R}_{mm'}(r) = \oint_r \Bigg\{ &\left[\frac{1}{2}\,(z - \cos\eta)^{-1/2}\, \hat{P}^n_{|m'|-1/2}(z) + (z - \cos\eta)^{1/2}\, \frac{d\hat{P}^n_{|m'|-1/2}}{dz}\right] \mathcal{J}\,\nabla r\cdot\nabla z \\ &+ \left[\frac{1}{2}\,(z - \cos\eta)^{-1/2}\, \sin\eta - \mathrm{i}\,m'\,(z - \cos\eta)^{1/2}\right] \hat{P}^n_{|m'|-1/2}(z)\, \mathcal{J}\,\nabla r\cdot\nabla\eta\Bigg\} \\ &\times \exp[-\mathrm{i}\,(m\,\theta + m'\,\eta)]\, \frac{d\theta}{2\pi}\end{aligned} \tag{C23}$$

values, $\underline{\underline{\mathcal{S}}}(r)$ is the matrix of the

$$\begin{aligned}\mathcal{S}_{mm'}(r) = \oint_r \Bigg\{ &\left[\frac{1}{2}\,(z - \cos\eta)^{-1/2}\, \hat{Q}^n_{|m'|-1/2}(z) + (z - \cos\eta)^{1/2}\, \frac{d\hat{Q}^n_{|m'|-1/2}}{dz}\right] \mathcal{J}\,\nabla r\cdot\nabla z \\ &+ \left[\frac{1}{2}\,(z - \cos\eta)^{-1/2}\, \sin\eta - \mathrm{i}\,m'\,(z - \cos\eta)^{1/2}\right] \hat{Q}^n_{|m'|-1/2}(z)\, \mathcal{J}\,\nabla r\cdot\nabla\eta\Bigg\} \\ &\times \exp[-\mathrm{i}\,(m\,\theta + m'\,\eta)]\, \frac{d\theta}{2\pi}\end{aligned} \tag{C24}$$

values, $\underline{p}$ is the vector of the p_m coefficients, and $\underline{q}$ is the vector of the q_m coefficients. Here, the subscript r on the integrals indicates that they are taken at constant r.

5. Toroidal Electromagnetic Torque

According to Eq. (B27), (B48), and Eq. (214) of Ref. 27, the net toroidal electromagnetic torque acting on the plasma is

$$T_\phi = -2\pi^2\, n\, \mathrm{Im}(\underline{V}^\dagger\, \underline{\psi}) = -\pi^2\, n\, (\underline{V}^\dagger\, \underline{\psi} - \underline{\psi}^\dagger\, \underline{V}). \tag{C25}$$

However, this torque must equal the flux of toroidal angular momentum into the vacuum region, so Eq. (C13) implies that

$$T_\phi = 2\pi^2\, n\, \mathrm{Im}(\underline{q}^\dagger\, \underline{p}) = \pi^2\, n\, (\underline{q}^\dagger\, \underline{p} - \underline{p}^\dagger\, \underline{q}). \tag{C26}$$

Now, Eqs. (C19), (C20), and (C25) give

$$\begin{aligned} T_\phi = -\pi^2\, n\, \Big[&\underline{p}^\dagger\, (\underline{\underline{\mathcal{P}}}^\dagger\, \underline{\underline{\mathcal{R}}} - \underline{\underline{\mathcal{R}}}^\dagger\, \underline{\underline{\mathcal{P}}})\, \underline{p} + \underline{p}^\dagger\, (\underline{\underline{\mathcal{P}}}^\dagger\, \underline{\underline{\mathcal{S}}} - \underline{\underline{\mathcal{R}}}^\dagger\, \underline{\underline{\mathcal{Q}}})\, \underline{q} \\ &-\underline{q}^\dagger\, (\underline{\underline{\mathcal{S}}}^\dagger\, \underline{\underline{\mathcal{P}}} - \underline{\underline{\mathcal{Q}}}^\dagger\, \underline{\underline{\mathcal{R}}})\, \underline{p} + \underline{q}^\dagger\, (\underline{\underline{\mathcal{Q}}}^\dagger\, \underline{\underline{\mathcal{S}}} - \underline{\underline{\mathcal{S}}}^\dagger\, \underline{\underline{\mathcal{R}}})\, \underline{q}\Big] \end{aligned} \tag{C27}$$

The previous equation is consistent with Eq. (C26) provided that

$$\underline{\underline{\mathcal{P}}}^\dagger\, \underline{\underline{\mathcal{R}}} = \underline{\underline{\mathcal{R}}}^\dagger\, \underline{\underline{\mathcal{P}}}, \tag{C28}$$

$$\underline{\underline{\mathcal{Q}}}^\dagger\, \underline{\underline{\mathcal{S}}} = \underline{\underline{\mathcal{S}}}^\dagger\, \underline{\underline{\mathcal{Q}}}, \tag{C29}$$

$$\underline{\underline{\mathcal{P}}}^\dagger\, \underline{\underline{\mathcal{S}}} - \underline{\underline{\mathcal{R}}}^\dagger\, \underline{\underline{\mathcal{Q}}} = \underline{\underline{1}}. \tag{C30}$$

The previous three equations can be combined with Eqs. (C19) and (C20) to give

$$\underline{p} = \underline{\underline{\mathcal{S}}}^{\,\dagger}\, \underline{V} - \underline{\underline{\mathcal{Q}}}^{\,\dagger}\, \underline{\psi}, \tag{C31}$$

$$\underline{q} = -\underline{\underline{\mathcal{R}}}^{\,\dagger}\, \underline{V} + \underline{\underline{\mathcal{P}}}^{\,\dagger}\, \underline{\psi}. \tag{C32}$$

However, the previous two equations are only consistent with Eqs. (C19) and (C20) provided

$$\underline{\underline{\mathcal{Q}}}\, \underline{\underline{\mathcal{P}}}^\dagger = \underline{\underline{\mathcal{P}}}\, \underline{\underline{\mathcal{Q}}}^\dagger, \tag{C33}$$

$$\underline{\underline{\mathcal{R}}}\, \underline{\underline{\mathcal{S}}}^\dagger = \underline{\underline{\mathcal{S}}}\, \underline{\underline{\mathcal{R}}}^\dagger, \tag{C34}$$

$$\underline{\underline{\mathcal{P}}}\, \underline{\underline{\mathcal{S}}}^\dagger - \underline{\underline{\mathcal{Q}}}\, \underline{\underline{\mathcal{R}}}^\dagger = \underline{\underline{1}}. \tag{C35}$$

Note that Eqs. (C28)–(C30) and (C33)–(C35) hold throughout the vacuum region.

6. Ideal-Wall Matching Condition

If the wall is perfectly conducting then $\underline{\psi}(b_w\, a) = 0$. It follows from Eq. (C20) that

$$\underline{q} = \underline{\underline{I}}_b\, \underline{p}, \tag{C36}$$

where

$$\underline{\underline{I}}_b = -\underline{\underline{\mathcal{S}}}_b^{-1}\, \underline{\underline{\mathcal{R}}}_b \tag{C37}$$

is termed the "wall matrix". Here, $\underline{\underline{\mathcal{S}}}_b = \underline{\underline{\mathcal{S}}}(b_w\, a)$, et cetera. Equation (C34) ensures that $\underline{\underline{I}}_b$ is Hermitian. It immediately follows from Eq. (C26) that $T_\phi = 0$. In other words, zero net toroidal electromagnetic torque is exerted on a plasma surrounded by a perfectly conducting wall. As described in Ref. 27, the fact that $T_\phi = 0$ ensures that the tearing stability matrix, $E_{kk'}$, introduced in Sect. A 6, is Hermitian.

Making use of Eqs. (C19) and (C20), the matching condition at the plasma-vacuum interface for a perfectly-conducting wall becomes

$$\underline{V}(a_+) = \underline{\underline{H}}\, \underline{\psi}(a), \tag{C38}$$

where

$$\underline{\underline{H}} = (\underline{\underline{\mathcal{P}}}_a + \underline{\underline{\mathcal{Q}}}_a\, \underline{\underline{I}}_b)\, (\underline{\underline{\mathcal{R}}}_a + \underline{\underline{\mathcal{S}}}_a\, \underline{\underline{I}}_b)^{-1} \tag{C39}$$

is the vacuum matrix introduced in Sect. B 11. Here, $\underline{\underline{\mathcal{P}}}_a = \underline{\underline{\mathcal{P}}}(a_+)$, et cetera. Making use of Eqs. (C28)–(C30), it is easily demonstrated that

$$\underline{\underline{H}} - \underline{\underline{H}}^\dagger = -[(\underline{\underline{\mathcal{R}}}_a + \underline{\underline{\mathcal{S}}}_a\, \underline{\underline{I}}_b)^{-1}]^\dagger\, (\underline{\underline{I}}_b - \underline{\underline{I}}_b^\dagger)\, (\underline{\underline{\mathcal{R}}}_a + \underline{\underline{\mathcal{S}}}_a\, \underline{\underline{I}}_b)^{-1} \tag{C40}$$

Thus, the vacuum matrix, $\underline{\underline{H}}$, is Hermitian because the wall matrix, $\underline{\underline{I}}_b$, is Hermitian.

7. Model Wall Matrix

Equations (C14)–(C18), (C23), and (C24) suggest that

$$\underline{\underline{\mathcal{R}}}_b = \underline{\underline{\mathcal{R}}}_a\, \underline{\underline{\rho}}^{-1}, \tag{C41}$$

$$\underline{\underline{\mathcal{S}}}_b = \underline{\underline{\mathcal{S}}}_a\, \underline{\underline{\rho}}, \tag{C42}$$

where

$$\rho_{mm'} = \delta_{mm'}\,\rho_m, \tag{C43}$$

$$\rho_0 = 1 + \ln b_w, \tag{C44}$$

$$\rho_{m\neq 0} = b_w^{|m|}. \tag{C45}$$

Hence,

$$\underline{\underline{I}}_b = -\underline{\underline{\rho}}^{-1\,\dagger}\,\underline{\underline{\mathcal{S}}}_a^{-1}\,\underline{\underline{\mathcal{R}}}_a\,\underline{\underline{\rho}}^{-1}. \tag{C46}$$

Note that our model wall matrix, $\underline{\underline{I}}_b$, is Hermitian given that $\underline{\underline{\mathcal{S}}}_a^{-1}\,\underline{\underline{\mathcal{R}}}_a$ is Hermitian. [See Eq. (C34).] Our model wall matrix allows us to smoothly interpolate between a plasma with no wall (which corresponds to $b_w \rightarrow \infty$ and $\underline{\underline{H}} = \underline{\underline{\mathcal{P}}}_a\,\underline{\underline{\mathcal{R}}}_a^{-1}$),[27] and a fixed boundary plasma (which corresponds to $b_w = 1$ and $\underline{\underline{H}}^{-1} = \underline{\underline{0}}$).

Appendix D: Resistive Layer Model

1. Introduction

The resistive layer model implemented in the TJ code is the three-field model described in Ref. 5. This model is a further development of the models derived in Refs. 3 and 4, and is ultimately based on the four-field model of Ref. 2. The model includes plasma resistivity, plasma inertia, electron and ion diamagnetic flows, the decoupling of ion and electron flows on lengthscales below the ion sound radius, and perpendicular momentum and energy transport. The three fields in the model are the (normalized) perturbed helical magnetic flux, ψ, the (normalized) perturbed electrostatic potential, ϕ, and the (normalized) perturbed electron number density, N. The model makes use of a low-β approximation that decouples the (normalized) parallel ion velocity, V, from the system of equations (thereby converting a four-field model into a three-field model). Reference 40 explains how the fourth field can be incorporated into the model. We choose not to do this because the fourth field is only important at high-β, and an aspect-ratio expanded equilibrium is, by definition, a relatively low-β equilibrium.

2. Plasma Parameters

The values of the following plasma parameters must be specified in order to calculate layer quantities:

- B_0 - the toroidal magnetic field-strength at the magnetic axis (T).
- R_0 - the major radius of the magnetic axis (m).
- n_0 - the electron number density at the magnetic axis (m^{-3}).
- α - the electron density profile is assumed to be $n_e(r) = n_0\,(1 - r^2/a^2)^\alpha$.
- $T_{e\,\mathrm{edge}}$ - the electron temperature at the plasma-vacuum interface (eV).
- Z_{eff} - the (assumed spatially uniform) effective ion charge number.
- M - the ion mass number.
- $\chi_\perp$ - the (assumed spatially uniform) perpendicular momentum/energy diffusivity.

3. Rational Surface Parameters

Let the kth rational surface lie at $r = r_k$, and possess the resonant poloidal mode number m_k. We can define $q_k = q(r_k)$, $s_k = s(r_k)$, $n_{e\,k} = n_0\,(1 - r_k^2/a^2)^\alpha$, $g_k = g(r_k)$,

$$p_k = \frac{B_0^2\,P(r_k),}{\mu_0} \tag{D1}$$

$$T_{e\,k} = \frac{p_k}{2\,n_{e\,k}\,e} + T_{e\,\mathrm{edge}}, \tag{D2}$$

$$\ln\Lambda_k = 24 + 3\,\ln 10 - \frac{1}{2}\ln n_{e\,k} + \ln T_{e\,k}, \tag{D3}$$

$$\tau_{ee\,k} = \frac{6\sqrt{2}\,\pi^{3/2}\,\epsilon_0^2\,m_e^{1/2}\,T_{e\,k}^{3/2}}{\ln\Lambda_k\,e^{5/2}\,n_{e\,k}}, \tag{D4}$$

$$\sigma_{\parallel\,k} = \frac{\sqrt{2} + 13\,Z_{\mathrm{eff}}/4}{Z_{\mathrm{eff}}\,(\sqrt{2} + Z_{\mathrm{eff}})}\,\frac{n_{e\,k}\,e^2\,\tau_{ee\,k}}{m_e}, \tag{D5}$$

$$L_{s\,k} = \frac{R_0\,q_k}{s_k}, \tag{D6}$$

$$V_{A\,k} = \frac{B_0\, g_k}{(\mu_0\, n_{e\,k}\, M\, m_p)^{1/2}}, \tag{D7}$$

$$d_{i\,k} = \left(\frac{M\, m_p}{n_{e\,k}\, e^2\, \mu_0}\right)^{1/2}, \tag{D8}$$

$$\beta_k = \frac{5\, P(r_k)}{3\, g_k^2}, \tag{D9}$$

$$\hat{d}_{\beta\,k} = \left(\frac{\beta_k}{1+\beta_k}\right)^{1/2} \frac{d_{i\,k}}{R_0\, r_k}, \tag{D10}$$

$$\omega_{*\,k} = \frac{m_k\, B_0}{\mu_0\, e\, n_{e\,k}\, R_0^2\, g_k\, r_k} \frac{dP(r_k)}{dr}, \tag{D11}$$

$$\tau_{H\,k} = \frac{L_{s\,k}}{m_k\, V_{A\,k}}, \tag{D12}$$

$$\tau_{R\,k} = \mu_0\, R_0^2\, r_k^2\, \sigma_{\parallel}(r_k), \tag{D13}$$

$$\tau_{\perp\,k} = \frac{R_0^2\, r_k^2}{\chi_\perp}, \tag{D14}$$

where e is the magnitude of the electron charge, m_e the electron mass, and m_p the proton mass. Note that we are assuming that the electrons and ions have the same temperature, as we would expect to be the case in a fusion reactor. Here, $d_{i\,k}$ is the collisionless skin-depth, $\hat{d}_{\beta\,k}$ the normalized ion sound radius, $\omega_{*\,k}$ the diamagnetic frequency, $\tau_{H\,k}$ the hydromagnetic timescale, $\tau_{R\,k}$ the resistive diffusion timescale, and $\tau_{\perp\,k}$ the perpendicular momentum/energy diffusion timescale, at the kth rational surface.

Layer physics at the kth rational surface is governed by the following normalized parameters: $\hat{\gamma}_k = \tau_k\, \gamma_k$, $Q_{e\,k} = -\tau_k\, \omega_{*\,k}/2$, $Q_{i\,k} = \tau_k\, \omega_{*\,k}/2$, $D_k = S_k^{1/3}\, \hat{d}_{\beta\,k}/\sqrt{2}$, and $P_k = \tau_{R\,k}/\tau_{\perp\,k}$, where $S_k = \tau_{R\,k}/\tau_{H\,k}$ and $\tau_k = S_k^{1/3}\, \tau_{H\,k}$. Here, S_k is the Lundquist number at the kth rational surface, and γ_k is the complex growth-rate of the tearing mode seen in the E-cross-B frame (i.e., a frame that co-rotates with the particle guiding centers) at the kth rational surface.

4. Resistive Layer Equations

The following resistive layer equations, which govern the response of the plasma at the kth rational surface to the ideal-MHD solution in the outer region, are obtained by linearizing

the three-field model of Ref. 5:

$$(\hat{\gamma}_k + \mathrm{i}\, Q_{e\,k})\,\psi = -\mathrm{i}\, X\,(\phi - N) + \frac{d^2\psi}{dX^2}, \tag{D15}$$

$$(\hat{\gamma}_k + \mathrm{i}\, Q_{i\,k})\,\frac{d^2\phi}{dX^2} = -\mathrm{i}\, X\,\frac{d^2\psi}{dX^2} + P_k\,\frac{d^4}{dX^4}(\phi + N)\,, \tag{D16}$$

$$\hat{\gamma}_k\, N = -\mathrm{i}\, Q_{e\,k}\,\phi - \mathrm{i}\, D_k^2\, X\,\frac{d^2\psi}{dX^2} + P_k\,\frac{d^2 N}{dX^2}, \tag{D17}$$

where $X = S_k^{1/3}\,(r - r_k)/r_k$. Here, it is assumed that $S_k \gg 1$. The asymptotic behavior of the tearing-parity [i.e., $\psi(-X) = \psi(X)$, $\phi(-X) = -\phi(X)$, and $N(-X) = -N(X)$] solution of the layer equations is such that

$$\psi(X) \rightarrow \psi_0\left[\frac{\hat{\Delta}_k}{2}\,|X| + 1 + \mathcal{O}\left(\frac{1}{X}\right)\right], \tag{D18}$$

$$\phi(X) \rightarrow \mathrm{i}\,\hat{\gamma}_k\,\psi_0\left[\frac{\hat{\Delta}_k}{2}\,\mathrm{sgn}(X) + \frac{1}{X} + \mathcal{O}\left(\frac{1}{X^2}\right)\right] \tag{D19}$$

as $|X| \rightarrow \infty$, where ψ_0 is an arbitrary constant, and $\hat{\Delta}_k = S_k^{-1/3}\,\Delta_k$. Here, Δ_k is the layer response parameter introduced in Sect. A 6.

5. Fourier Transformation

Equations (D15)–(D17) are most conveniently solved in Fourier transform space.[4] Let

$$\hat{\phi}(p) = \int_{-\infty}^{\infty} \phi(X)\,\mathrm{e}^{-\mathrm{i}\,p\,X}\,dX, \tag{D20}$$

et cetera. The Fourier transformed linear layer equations become

$$(\hat{\gamma}_k + \mathrm{i}\, Q_{e\,k})\,\hat{\psi} = \frac{d}{dp}\Big(\hat{\phi} - \hat{N}\Big) - p^2\,\hat{\psi}, \tag{D21}$$

$$(\hat{\gamma}_k + \mathrm{i}\, Q_{i\,k})\,p^2\,\hat{\phi} = \frac{d(p^2\,\hat{\psi})}{dp} - P_k\,p^4\,(\hat{\phi} + \hat{N}), \tag{D22}$$

$$\hat{\gamma}_k\,\hat{N} = -\mathrm{i}\, Q_{e\,k}\,\hat{\phi} - D_k^2\,\frac{d(p^2\,\hat{\psi})}{dp} - P_k\,p^2\hat{N}, \tag{D23}$$

where, for a tearing-parity solution, Eq. (D19) yields [41]

$$\hat{\phi}(p) = \pi\,\hat{\gamma}_k\,\psi_0\left[\frac{\hat{\Delta}_k}{\pi\,p} + 1 + \mathcal{O}(p)\right] \tag{D24}$$

as $p \to 0$.

Let

$$Y_e(p) \equiv \hat{\phi}(p) - \hat{N}(p) = \pi\,(\hat{\gamma}_k + \mathrm{i}\,Q_{e\,k})\,\psi_0\,\hat{Y}_e(p). \tag{D25}$$

Equations (D21)–(D23) can be combined to give [4,5]

$$\frac{d}{dp}\left[A(p)\,\frac{d\hat{Y}_e}{dp}\right] - \frac{B(p)}{C(p)}\,p^2\,\hat{Y}_e = 0, \tag{D26}$$

where

$$A(p) = \frac{p^2}{\hat{\gamma}_k + \mathrm{i}\,Q_{e\,k} + p^2}, \tag{D27}$$

$$B(p) = \hat{\gamma}_k\,(\hat{\gamma}_k + \mathrm{i}\,Q_{i\,k}) + 2\,(\hat{\gamma}_k + \mathrm{i}\,Q_{i\,k})\,P_k\,p^2 + P_k^2\,p^4, \tag{D28}$$

$$C(p) = \hat{\gamma}_k + \mathrm{i}\,Q_{e\,k} + [P_k + (\hat{\gamma}_k + \mathrm{i}\,Q_{i\,k})\,D_k^2]\,p^2 + 2\,P_k\,D_k^2\,p^4. \tag{D29}$$

Because

$$Y_e(p) = \frac{(\hat{\gamma}_k + \mathrm{i}\,Q_{e\,k})}{\hat{\gamma}_k}\,\hat{\phi} \tag{D30}$$

as $p \to 0$, Eqs. (D24) and (D25) yield the following small-p boundary condition that Eq. (D26) must satisfy:

$$\hat{Y}_e(p) \to \frac{\hat{\Delta}_k}{\pi\,p} + 1 + \mathcal{O}(p) \tag{D31}$$

as $p \to 0$. Equation (D26) must also satisfy the physical boundary condition

$$\hat{Y}_e(p) \to 0 \tag{D32}$$

as $p \to \infty$. In fact, in the large-p/large-D_k limit, $p \gg 1$ and $D_k \gg P_k^{1/6}$, the well-behaved solution of Eq. (D26) takes the form

$$\hat{Y}_e(p) = Y_0\,p^{\,x_k}\,\exp\left(\frac{-\sqrt{b_k}\,p^2}{2}\right) \tag{D33}$$

where Y_0 is independent of p, and

$$x_k = \frac{c_k - \sqrt{b_k}\,(1 - \sqrt{b_k}\,a_k)}{2\sqrt{b_k}}, \tag{D34}$$

$$a_k = -(\hat{\gamma}_k + \mathrm{i}\,Q_{e\,k}), \tag{D35}$$

$$b_k = \frac{P_k}{2\,D_k^2}, \tag{D36}$$

$$c_k = \frac{P_k}{2\,D_k^2}\left[1 + \frac{2\,(\hat{\gamma}_k + \mathrm{i}\,Q_{i\,k})}{P_k} - \frac{(P_k + [\hat{\gamma}_k + \mathrm{i}\,Q_{i\,k}]\,D_k^2)}{2\,P_k\,D_k^2}\right]. \tag{D37}$$

On the other hand, in the large-p/small-D_k limit, $p \gg 1$ and $D_k \ll P_k^{1/6}$, the well-behaved solution of Eq. (D26) is

$$\hat{Y}_e(p) = Y_0\,p^{-1}\,\exp\left(x_k\,p - \frac{\sqrt{b_k}\,p^3}{3}\right), \tag{D38}$$

where

$$x_k = \frac{a_k\,b_k - c_k}{2\sqrt{b_k}}, \tag{D39}$$

$$a_k = -(\hat{\gamma}_k + \mathrm{i}\,Q_{e\,k}), \tag{D40}$$

$$b_k = P_k, \tag{D41}$$

$$c_k = -\mathrm{i}\,(Q_{e\,k} - Q_{i\,k}) + (\hat{\gamma}_k + \mathrm{i}\,Q_{i\,k}). \tag{D42}$$

6. Ricatti Transformation

Equation (D26) is most conveniently solved by means of a Ricatti transformation.[42,43] Let

$$W(p) = \frac{p}{\hat{Y}_e}\,\frac{d\hat{Y}_e}{dp}. \tag{D43}$$

Equation (D26) transforms to give

$$\frac{dW}{dp} = -\frac{A'}{p}\,W - \frac{W^2}{p} + \frac{B}{A\,C}\,p^3, \tag{D44}$$

where

$$A' = \frac{\hat{\gamma}_k + \mathrm{i}\,Q_{e\,k} - p^2}{\hat{\gamma}_k + \mathrm{i}\,Q_{e\,k} + p^2}. \tag{D45}$$

According to Eqs. (D31), (D33), and (D38), this equation must be solved subject to the boundary condition that

$$W(p) = x_k - \sqrt{b_k}\,p^2 \tag{D46}$$

at large p and large D_k, or

$$W(p) = -1 + x_k\,p - \sqrt{b_k}\,p^3 \tag{D47}$$

at large p and small D_k, and

$$W(p) = -1 + \frac{\pi\, p}{\hat{\Delta}_k} \tag{D48}$$

at small p. The method of solution is to launch a solution of Eq. (D44) from large p, subject to the boundary condition (D46) or (D47), as appropriate, and integrate it to small p. We can then deduce the value of $\hat{\Delta}_k$ from Eq. (D48).

Appendix E: Asymptotic Matching Between Outer and Inner Regions

1. Introduction

Consider the segment of the inner region that is centered on the kth rational surface. Let the surface lie at $r = r_k$, and possess the resonant poloidal mode number m_k. According to Sect. A 5, in the limit $r \to r_k$, the asymptotic behavior of the resonant tearing-parity component of the perturbed helical magnetic flux, ψ, [see Eq. (A3)] in the outer region is

$$\psi_{m_k}(x) = A_{L\,k}\,|x|^{-\nu_k} + A_{S\,k}\,|x|^{\,1+\nu_k}, \tag{E1}$$

where $x = r - r_k$, $\nu_k = -1/2 + \sqrt{-D_{I\,k}}$, and

$$\Delta_k = \frac{2\, r_k^{1+2\,\nu_k}\, A_{S\,k}}{A_{L\,k}}. \tag{E2}$$

Here, $D_{I\,k}$ is the ideal interchange parameter defined in Eq. (A10), and Δ_k is the layer response parameter that appears in the tearing mode dispersion relation, (A17). On the other hand, according to Sect. D 4, the asymptotic behavior of the resistive layer solution in the segment of the inner region, as it approaches the outer region, is

$$\psi_{m_k}(x) = B_{L\,k} + B_{S\,k}\,|x|, \tag{E3}$$

where

$$\Delta_k = \frac{2\, r_k\, B_{S\,k}}{B_{L\,k}}. \tag{E4}$$

It can be seen that the solutions (E1) and (E3) only match if $\nu_k = 0$. The reason for the mismatch is because the outer solution takes average magnetic field-line curvature into account,[35,36] whereas the layer solution does not. The aim of this appendix is to describe a method for resolving the mismatch.

2. Pressure Flattening

In the immediate vicinity of the rational surface, the equation that governs the resonant component of ψ in the outer region reduces to [27]

$$\frac{d^2\psi_{m_k}}{dx^2} = \frac{\nu_k\,(1+\nu_k)}{x^2}\,\psi_{m_k}, \tag{E5}$$

where

$$\nu_k\,(1+\nu_k) = -D_{I\,k} - \frac{1}{4} = \left[\frac{2\,(1-q^2)}{s^2}\,r\,\frac{dP}{dr}\right]_{r_k}. \tag{E6}$$

Following Ref. 44, let us suppose that the pressure gradient is locally flattened in the vicinity of the rational surface in such a manner that

$$\frac{dP}{dx} = \left(\frac{dP}{dr}\right)_{r_k}\,\frac{x^2}{x^2+\delta_k^2}. \tag{E7}$$

Here, it is assumed that $\delta_k \ll r_k$. Equation (E5) transforms to give

$$(1+X^2)\,\frac{d^2\psi_{m_k}}{dX^2} = \nu_k\,(1+\nu_k)\,\psi_{m_k}, \tag{E8}$$

where $X = x/\delta_k$.

The most general tearing-parity solution of Eq. (E8) in the limit $|X| \rightarrow 0$ takes the form

$$\psi_{m_k}(X) \simeq \hat{B}_{L\,k} + \hat{B}_{S\,k}\,|X|. \tag{E9}$$

We can define

$$\Delta_{k\,\rm in} = \left(\frac{r_k}{\delta_k}\right)\frac{2\,\hat{B}_{S\,k}}{\hat{B}_{L\,k}}. \tag{E10}$$

On the other hand, the most general tearing-parity solution of Eq. (E8) in the limit $|X| \rightarrow \infty$ is written

$$\psi_{m_k}(X) = \hat{A}_{L\,k}\,|X|^{-\nu_k} + \hat{A}_{S\,k}\,|X|^{1+\nu_k}. \tag{E11}$$

We can define

$$\Delta_{k\,\rm out} = \left(\frac{r_k}{\delta_k}\right)^{1+2\,\nu_k}\,\frac{2\,\hat{A}_{S\,k}}{\hat{A}_{L\,k}}. \tag{E12}$$

A comparision between Eqs. (E1)–(E4) and (E9)–(E12) reveals that the solution to Eq. (E8) successfully interpolates between the resistive layer solution and the outer solution. It now remains to determine the relationship between $\Delta_{k\,\rm in}$ and $\Delta_{k\,\rm out}$.

3. Connection Formula

Suppose that we launch a "large" solution of Eq. (E8), $\psi_L(X) = X^{-\nu_k}$, from large X, and integrate to $X = 0$. Let

$$\psi_L(0) = a_{LL}, \tag{E13}$$

$$\frac{d\psi_L(0)}{dx} = a_{SL}. \tag{E14}$$

Next, suppose that we launch a "small" solution, $\psi_S(X) = X^{1+\nu_k}$, from large X, and integrate to $X = 0$. Let

$$\psi_S(0) = a_{LS}, \tag{E15}$$

$$\frac{d\psi_S(0)}{dx} = a_{SS}. \tag{E16}$$

The most general solution is

$$\psi_{m_k}(X) = \hat{A}_{L\,k}\,\psi_L(X) + \hat{A}_{S\,k}\,\psi_S(X). \tag{E17}$$

It follows that

$$\hat{B}_{L\,k} = a_{LL}\,\hat{A}_{L\,k} + a_{LS}\,\hat{A}_{S\,k}, \tag{E18}$$

$$\hat{B}_{S\,k} = a_{SL}\,\hat{A}_{L\,k} + a_{SS}\,\hat{A}_{S\,k}. \tag{E19}$$

Thus, Eqs. (E10) and (E12) yield the connection formula

$$\left(\frac{\delta_k}{r_k}\right)\frac{\Delta_{k\,\rm in}}{2} = \frac{a_{SL} + a_{SS}\,(\delta_k/r_k)^{1+2\,\nu_k}\,(\Delta_{k\,\rm out}/2)}{a_{LL} + a_{LS}\,(\delta_k/r_k)^{1+2\,\nu_k}\,(\Delta_{k\,\rm out}/2)}. \tag{E20}$$

It remains to calculate the coefficients a_{LL}, a_{LS}, a_{SL}, and a_{SS}.

4. Analytic Solution

Let $\psi_{m\,k} = (1 + X^2)\,\phi$ and $z = {\rm i}\,X$. Equation (E8) transforms to give

$$(1 - z^2)\,\frac{d^2\phi}{dz^2} - 4\,z\,\frac{d\phi}{dz} - [2 - \nu_k\,(1 + \nu_k)]\,\phi = 0. \tag{E21}$$

Now, the Legendre functions $Q_{\nu_k}(z)$ and $Q_{-1-\nu_k}(z)$ satisfy [45]

$$(1-z^2)\,\frac{d^2w}{dz^2} - 2\,z\,\frac{dw}{dz} + \nu_k\,(1+\nu_k)\,w = 0. \tag{E22}$$

Let $w' = dw/dz$. Differentiation of the previous equation yields

$$(1-z^2)\,\frac{d^2w'}{dz^2} - 4\,z\,\frac{dw'}{dz} - [2-\nu_k\,(1+\nu_k)]\,w' = 0. \tag{E23}$$

It is clear from a comparison of Eqs. (E21) and (E23) that the two independent solutions of Eq. (E8) can be written $(1+X^2)\,Q'_{\nu_k}(\mathrm{i}\,X)$ and $(1+X^2)\,Q'_{-1-\nu_k}(\mathrm{i}\,X)$, where $'$ denotes differentiation with respect to argument.

Now,[46]

$$\begin{aligned} Q_{\nu_k}(z) = {} & \frac{\pi^{1/2}\,\Gamma(1/2+\nu_k/2)\,\mathrm{e}^{-\mathrm{i}\,(\pi/2)\,(1+\nu_k)}}{2\,\Gamma(1+\nu_k/2)}\,F\left(-\frac{\nu_k}{2},\frac{1}{2}+\frac{\nu_k}{2};\frac{1}{2};z^2\right) \\ & + \frac{\pi^{1/2}\,\Gamma(1+\nu_k/2)\,\mathrm{e}^{-\mathrm{i}\,(\pi/2)\,\nu_k}}{\Gamma(1/2+\nu_k/2)}\,z\,F\left(\frac{1}{2}-\frac{\nu_k}{2},1+\frac{\nu_k}{2};\frac{3}{2};z^2\right), \end{aligned} \tag{E24}$$

where $F(a,b;c;z)$ is a hypergeometric function and $\Gamma(z)$ is a gamma function,[38,47] which yields

$$\begin{aligned} Q'_{\nu_k}(z) \simeq {} & \frac{\pi^{1/2}\,\Gamma(1+\nu_k/2)\,\mathrm{e}^{-\mathrm{i}\,(\pi/2)\,\nu_k}}{\Gamma(1/2+\nu_k/2)} \\ & - \frac{\pi^{1/2}\,\nu_k\,(1+\nu_k)\,\Gamma(1/2+\nu_k/2)\,\mathrm{e}^{-\mathrm{i}\,(\pi/2)\,(1+\nu_k)}}{2\,\Gamma(1+\nu_k/2)}\,z + \mathcal{O}(z^2). \end{aligned} \tag{E25}$$

So, at small X,

$$(1+X^2)\,Q'_{\nu_k}(\mathrm{i}\,X) \simeq \mathrm{e}^{-\mathrm{i}\,\nu_k\,\pi/2}\left[\frac{\pi^{1/2}\,\Gamma(1+\nu_k/2)}{\Gamma(1/2+\nu_k/2)} - \frac{\pi^{1/2}\,\nu_k\,(1+\nu_k)\,\Gamma(1/2+\nu_k/2)}{2\,\Gamma(1+\nu_k/2)}\,X\right]. \tag{E26}$$

Furthermore,[46]

$$Q_{\nu_k}(z) = \frac{\pi^{1/2}\,\Gamma(1+\nu_k)}{2^{1+\nu_k}\,\Gamma(3/2+\nu_k)}\,z^{-1-\nu_k}\,F\left(1+\frac{\nu_k}{2},\frac{1}{2}+\frac{\nu_k}{2};\frac{3}{2}+\nu_k;\frac{1}{z^2}\right), \tag{E27}$$

which yields

$$Q'_{\nu_k}(z) \simeq -\frac{\pi^{1/2}\,(1+\nu_k)\,\Gamma(1+\nu_k)}{2^{1+\nu_k}\,\Gamma(3/2+\nu_k)}\,z^{-2-\nu_k} + \mathcal{O}(z^{-4-\nu_k}) \tag{E28}$$

So, at large X,

$$(1+X^2)\,Q'_{\nu_k}(\mathrm{i}\,X) \simeq \mathrm{e}^{-\mathrm{i}\,\nu_k\,\pi/2}\,\frac{\pi^{1/2}\,(1+\nu_k)\,\Gamma(1+\nu_k)}{2^{1+\nu_k}\,\Gamma(3/2+\nu_k)}\,X^{-\nu_k}. \tag{E29}$$

It is clear from a comparison of Eqs. (E9), (E11), (E18), (E19), (E26), and (E29) that $\hat{B}_{L\,k} = a_{LL}\,\hat{A}_{L\,k}$ and $\hat{B}_{S\,k} = a_{SL}\,\hat{A}_{L\,k}$, where

$$a_{LL} = \frac{2^{1+\nu_k}\,\Gamma(1+\nu_k/2)\,\Gamma(3/2+\nu_k)}{(1+\nu_k)\,\Gamma(1/2+\nu_k/2)\,\Gamma(1+\nu_k)}, \tag{E30}$$

$$a_{SL} = -\frac{2^{\nu_k}\,\nu_k\,\Gamma(1/2+\nu_k/2)\,\Gamma(3/2+\nu_k)}{\Gamma(1+\nu_k/2)\,\Gamma(1+\nu_k)}. \tag{E31}$$

In the limit $\nu_k \to 0$,

$$a_{LL} \to 1, \tag{E32}$$

$$a_{SL} \to -\frac{\nu_k\,\pi}{2}. \tag{E33}$$

Now, according to Eq. (E26),

$$(1+X^2)\,Q'_{-1-\nu_k}(\mathrm{i}\,X) \simeq \mathrm{e}^{\,\mathrm{i}\,(1+\nu_k)\,\pi/2}\left[\frac{\pi^{1/2}\,\Gamma(1/2-\nu_k/2)}{\Gamma(-\nu_k/2)} - \frac{\pi^{1/2}\,\nu_k\,(1+\nu_k)\,\Gamma(-\nu_k/2)}{2\,\Gamma(1/2-\nu_k/2)}\,X\right] \tag{E34}$$

at small X. Furthermore, according to Eq. (E29),

$$(1+X^2)\,Q'_{-1-\nu_k}(\mathrm{i}\,X) \simeq -\mathrm{e}^{\,\mathrm{i}\,(1+\nu_k)\,\pi/2}\,\frac{\pi^{1/2}\,\nu_k\,\Gamma(-\nu_k)}{2^{-\nu_k}\,\Gamma(1/2-\nu_k)}\,X^{1+\nu_k} \tag{E35}$$

at large X. A comparison of Eqs. (E9), (E11), (E18), (E19), (E34), and (E35) yields $\hat{B}_{L\,k} = a_{LS}\,\hat{A}_{S\,k}$ and $\hat{B}_{S\,k} = a_{SS}\,\hat{A}_{S\,k}$, where

$$a_{LS} = -\frac{\nu_k\,\Gamma(1/2-\nu_k/2)\,\Gamma(1/2-\nu_k)}{2^{1+\nu_k}\,\Gamma(1-\nu_k)\,\Gamma(1-\nu_k/2)}, \tag{E36}$$

$$a_{SS} = \frac{(1+\nu_k)\,\Gamma(1-\nu_k/2)\,\Gamma(1/2-\nu_k)}{2^{\nu_k}\,\Gamma(1/2-\nu_k/2)\,\Gamma(1-\nu_k)}. \tag{E37}$$

In the limit $\nu_k \to 0$,

$$a_{LS} \to -\frac{\nu_k\,\pi}{2}, \tag{E38}$$

$$a_{SS} \to 1. \tag{E39}$$

5. Matching Formula

A large aspect-ratio tokamak equilibrium is characterized by $|\nu_k| \ll 1$. In this limit, Eqs. (E20) (E32), (E33), (E38), and (E39) yield

$$\Delta_{k\,\rm out} = \Delta_{k\,\rm in} + \frac{\pi\,\nu_k\,r_k}{\delta_k}. \tag{E40}$$

It remains to specify the pressure-flattening width, δ_k. Following Refs. 48 and 49, we identify this width with the critical layer width above which parallel thermal transport forces the electron temperature to be a flux-surface function. This critical layer width is given by [50,51]

$$\delta_{d\,k} = \sqrt{8}\left(\frac{\chi_\perp}{\chi_\parallel}\right)^{1/4}\frac{r_k}{(r_k\,s_k\,n)^{1/2}}, \tag{E41}$$

$$\chi_\parallel = \frac{\chi_\parallel^{\rm smfp}\,\chi_\parallel^{\rm lmfp}}{\chi_\parallel^{\rm smfp}+\chi_\parallel^{\rm lmfp}}, \tag{E42}$$

$$\chi_\parallel^{\rm smfp} = \frac{1.581\,\tau_{ee\,k}\,v_{t\,e\,k}^2}{1+0.2535\,Z_{\rm eff}}, \tag{E43}$$

$$\chi_\parallel^{\rm lmfp} = \frac{2\,R_0\,v_{t\,e\,k}\,r_k}{\pi^{1/2}\,n\,s_k\,\delta_{d\,k}}, \tag{E44}$$

$$v_{t\,e\,k} = \left(\frac{2\,T_{e\,k}}{m_e}\right)^{1/2}. \tag{E45}$$

The previous five equations can be solved via iteration. In fact, if we choose $\delta_k = \delta_{d\,k}/(2\sqrt{\pi})$, identify $\Delta_{k\,\rm out}$ with the Δ_k appearing in the tearing mode dispersion relation (A17), identify $\Delta_{k\,\rm in}$ with the $S_k^{1/3}\,\hat{\Delta}_k$ obtained from the solution of the layer equations (see Appendix. D), and identify ν_k with minus the resistive interchange stability parameter,[35,36]

$$D_{R\,k} = \left(\frac{2\,q^2}{s^2}\,r\,\frac{dP}{dr}\right)_{r_k}\left[1-\frac{1}{q_k^2}+\frac{q_k^2\,s_k}{r_k^4}\int_0^{r_k}\left(\frac{r^3}{q^2}-2\,R_0^2\,r^2\,\frac{dP}{dr}\right)dr\right] \tag{E46}$$

[rather than $-D_{I\,k}-1/4$—see Eq. (E6)],[52] then we obtain

$$\Delta_k = S_k^{1/3}\,\hat{\Delta}_k - \sqrt{2}\,\pi^{3/2}\,D_{R\,k}\,\frac{r_k}{\delta_{d\,k}}. \tag{E47}$$

This formula reproduces one given (but, unfortunately, not derived) in Ref. 48 that has been successfully benchmarked against the XTOR code. The final term on the right-hand side of

the previous equation represents the stabilizing effect of average magnetic field-line curvature on tearing modes in tokamak plasmas.

It should be understood that the local flattening of the pressure profile considered in this section is not real, but rather a proxy for modeling the influence of large parallel thermal conductivity on the so-called Glasser curvature stabilization term.[35,36,49] Furthermore, the neglect of parallel transport in the resistive layer model described in Appendix D is justified on the assumption that the layer width is much less than the flattening width, δ_k.

Appendix F: Comparison between TJ and STRIDE Codes

Suppose that there are K rational surfaces in the plasma. The TJ toroidal tearing stability code calculates a K-dimensional square tearing stability matrix whose elements are denoted $E_{kk'}$, for $k, k' = 1, K$, from the ideal-MHD solution in the outer region.[27] Similarly, the STRIDE toroidal tearing mode stability code calculates a K-dimensional square tearing stablility matrix whose elements are denoted $\Delta_{kk'}$, for $k, k' = 1, K$.[22] As described in Ref. 27, the $E_{kk'}$ matrix is necessarily Hermitian, otherwise toroidal electromagnetic angular momentum would not be conserved. On the other hand, the $\Delta_{kk'}$ matrix is not generally Hermitian. (Note that it was originally appreciated that the $\Delta_{kk'}$ matrix must satisfy certain symmetry requirements,[11] but this requirement was forgotten over the years.) Fortunately, it is possible to transform the $\Delta_{kk'}$ into an Hermitian matrix, whose elements are denoted $\hat{\Delta}_{kk'}$, that is equivalent to the $E_{kk'}$ matrix calculated by the TJ code.

The normalized equilibrium poloidal magnetic flux is defined as $\Psi(r) = \int_0^r f(r')\,dr'$. Let $\Psi_a = \Psi(a)$ be the total flux enclosed in the plasma. If

$$\rho(r) = \frac{r\,f}{\Psi_a}, \tag{F1}$$

$$f_{L\,k} = \left[\rho^{\nu_{L\,k}-1}\left(\frac{\nu_{S\,k}-\nu_{L\,k}}{L_{m_k}^{m_k}}\right)^{1/2} s\,m_k\,\Psi_a\right]_{r_k}, \tag{F2}$$

$$f_{S\,k} = \left[\rho^{\nu_{S\,k}-1}\left(\frac{\nu_{S\,k}-\nu_{L\,k}}{L_{m_k}^{m_k}}\right)^{1/2} s\,m_k\,\Psi_a\right]_{r_k}, \tag{F3}$$

where all quantities are defined in Sects. A 2, A 3, and A 5, then

$$\hat{\Delta}_{kk'} = \cos[(k+k')\,\pi]\, f_{S\,k}\, \Delta_{kk'}/f_{L\,k'}. \tag{F4}$$

Note that the STRIDE calculation must be performed with PEST coordinates (because these are the coordinates used by TJ). Finally, the STRIDE code needs to be run using the following non-default parameters: `tol_r` = `tol_nr` = 10^{-12} and `sas_flag` = `False`.

---

[1] H.P. Furth, J. Killeen and M.N. Rosenbluth, Phys. Fluids **6**, 459 (1963).

[2] R.D. Hazeltine, M. Kotschenreuther and P.G. Morrison, Phys. Fluids **2**, 2466 (1985).

[3] R. Fitzpatrick and F.L. Waelbroeck, Phys. Plasmas **12**, 022307 (2005).

[4] A. Cole and R. Fitzpatrick, Phys. Plasmas **13**, 032503 (2006).

[5] R. Fitzpatrick, Phys. Plasmas **29**, 032507 (2022).

[6] J.W. Connor and R.J. Hastie, *The Effect of Shaped Plasma Cross Sections on the Ideal Kink Mode in a Tokamak* (Rep. CLM-M106, Culham Laboratory, Abingdon UK, 1985).

[7] J.W. Connor, R.J. Hastie and J.B. Taylor, Phys. Fluids B **3**, 1539 (1991).

[8] J.W. Connor, S.C. Cowley, R.J. Hastie, T.C. Hender, A. Hood and T.J. Martin, Phys. Fluids **31**, 577 (1988).

[9] A. Pletzer and R.L. Dewar, J. Plasma Physics **45**, 427 (1991).

[10] R. Fitzpatrick, R.J. Hastie, T.J. Martin and C.M. Roach, Nucl. Fusion **33**, 1533 (1993).

[11] A. Pletzer, A. Bondeson and R.L. Dewar, J. Comput. Phys. **115**, 530 (1994).

[12] Y. Nishimura, J.D. Callen and C.C. Hegna, Phys. Plasmas **5**, 4292 (1998).

[13] S.A. Galkin, A.D. Turnbull, J.M. Greene and M.S. Chu, Phys. Plasmas **7**, 4070 (2000).

[14] S. Tokuda, Nucl. Fusion **41**, 1037 (2001).

[15] D.P. Brennan, R.J. La Haye, A.D. Turnbull, M.S. Chu, T.H. Jensen, L.L. Lao, T.C. Luce, P.A. Politzer, E.J. Strait, S.E. Kruger and D.D. Schnack, Phys. Plasmas **10**, 1643 (2003).

[16] C.J. Ham, Y.Q. Liu, J.W. Connor, S.C. Cowley, R.J. Hastie, T.C. Hender and T.J. Martin,

Plasma Phys. Controlled Fusion **54**, 105014 (2012).

[17] C.J. Ham, J.W. Connor, S.C. Cowley, C.G. Gimblett, R.J. Hastie, T.C. Hender and T.J. Martin, Plasma Phys. Controlled Fusion **54**, 025009 (2012).

[18] C.J. Ham, J.W. Connor, S.C. Cowley, R.J. Hastie, T.C. Hender and Y.Q. Liu, Plasma Phys. Control. Fusion **55** 125015 (2013).

[19] A.H. Glasser, Z.R. Wang and J.-K. Park, Phys. Plasmas **23**, 112506 (2016).

[20] R. Fitzpatrick, Phys. Plasmas **24**, 072506 (2017).

[21] A.S. Glasser, E. Kolemen and A.H. Glasser, Phys. Plasmas **25**, 032507 (2018).

[22] A.S. Glasser and E. Koleman, Phys. Plasmas **25**, 082502 (2018).

[23] Z. Wang, A.H. Glasser, D. Brennan, Y. Liu and J.-K. Park, Phys. Plasmas **27**, 122503 (2020).

[24] J.M. Greene, J.L. Johnson and K.E. Weimer, Phys. Fluids **14**, 671 (1971).

[25] R. Fitzpatrick, C.G. Gimblett and R.J. Hastie, Plasma Phys. Control. Fusion **34**, 161 (1992).

[26] R. Fitzpatrick, Phys. Plasmas **31**, 082505 (2024).

[27] R. Fitzpatrick, Phys. Plasmas **31**, 102507 (2024).

[28] D.P. Brennan, E.J. Strait, D. Turnbull, M.S. Chu, R.J. La Haye, T.C. Luce, T.S. Taylor, S. Kruger and A. Pletzer, Phys. Plasmas **9**, 2998 (2002).

[29] D.P. Brennan, A.D. Turnbull, M.S. Chu, R.J. La Haye, L.L. Lao, T.H. Osborne and S.A. Galkin, Phys. Plasmas **14**, 056108 (2007).

[30] J.P. Freidberg, Rev. Mod. Phys. **54**, 801 (1982).

[31] R. Fitzpatrick, Phys. Plasmas **31**, 112502 (2024).

[32] A.H. Glasser, Phys. Plasmas **23**, 072505 (2016).

[33] J.-K. Park, A.H. Boozer and A.H. Glasser, Phys. Plasmas **14**, 52110 (2007).

[34] C. Mercier, Nucl. Fusion **1**, 47 (1960).

[35] A.H. Glasser, J.M. Greene and J.L. Johnson, Phys. Fluids **18**, 875 (1975).

[36] A.H. Glasser, J.M. Greene and J.L. Johnson, Phys. Fluids **19**, 567 (1976).

[37] M. Abramowitz and I.A. Stegun, *Handbook of Mathematical Functions* (Dover, New York NY,

1964), sect. 8.11.

[38] M. Abramowitz and I.A. Stegun, *Handbook of Mathematical Functions* (Dover, New York NY, 1964), ch. 6.

[39] P.M. Morse and H. Feshbach, *Methods of Theoretical Physics* (McGraw-Hill, New York NY, 1953), pp. 1302–1329.

[40] Y. Lee, J.-K. Park and Y.-S. Na, Nucl. Fusion **64**, 106058 (2024).

[41] A. Erdélyi, W. Magnus, F. Oberhettinger and F.G. Tricomi, *Tables of Integral Transforms*, Vol. 1. (McGraw-Hill, New York NY, 1954).

[42] D.P. Brennan, A.J. Cole, C. Akcay and J.M. Finn, Bul. Am. Phys. Soc. **64**, 249 (2019).

[43] J.-K. Park, Phys. Plasmas **29**, 072506 (2022).

[44] C.M. Bishop, J.W. Connor, R.J. Hastie and S.C. Cowley, Plasma Phys. Control. Fusion **33**, 389 (1991).

[45] M. Abramowitz and I.A. Stegun, *Handbook of Mathematical Functions* (Dover, New York NY, 1964), ch. 8.

[46] A. Erdélyi, W. Magnus, F. Oberhettinger and F.G. Tricomi, *Higher Trancendental Functions*, Vol. 1. (McGraw-Hill, New York NY, 1954), p. 134.

[47] M. Abramowitz and I.A. Stegun, *Handbook of Mathematical Functions* (Dover, New York NY, 1964), ch. 15.

[48] H. Lütjens, J.-F. Luciani and X. Garbet, Phys. Plasmas **8**, 4267 (2001).

[49] J.W. Connor, C.J. Ham, R.J. Hastie and Y.Q. Liu, Plasma Phys. Control. Fusion **57**, 065001 (2015).

[50] R. Fitzpatrick, Phys. Plasmas **2**, 825 (1995).

[51] R. Fitzpatrick, R. Maingi, J.-K. Park and S. Sabbagh, Phys. Plasmas **30**, 072505 (2023).

[52] M. Kotschenreuther, R.D. Hazeltine and P.J. Morrison, Phys. Fluids **28**, 294 (1985).

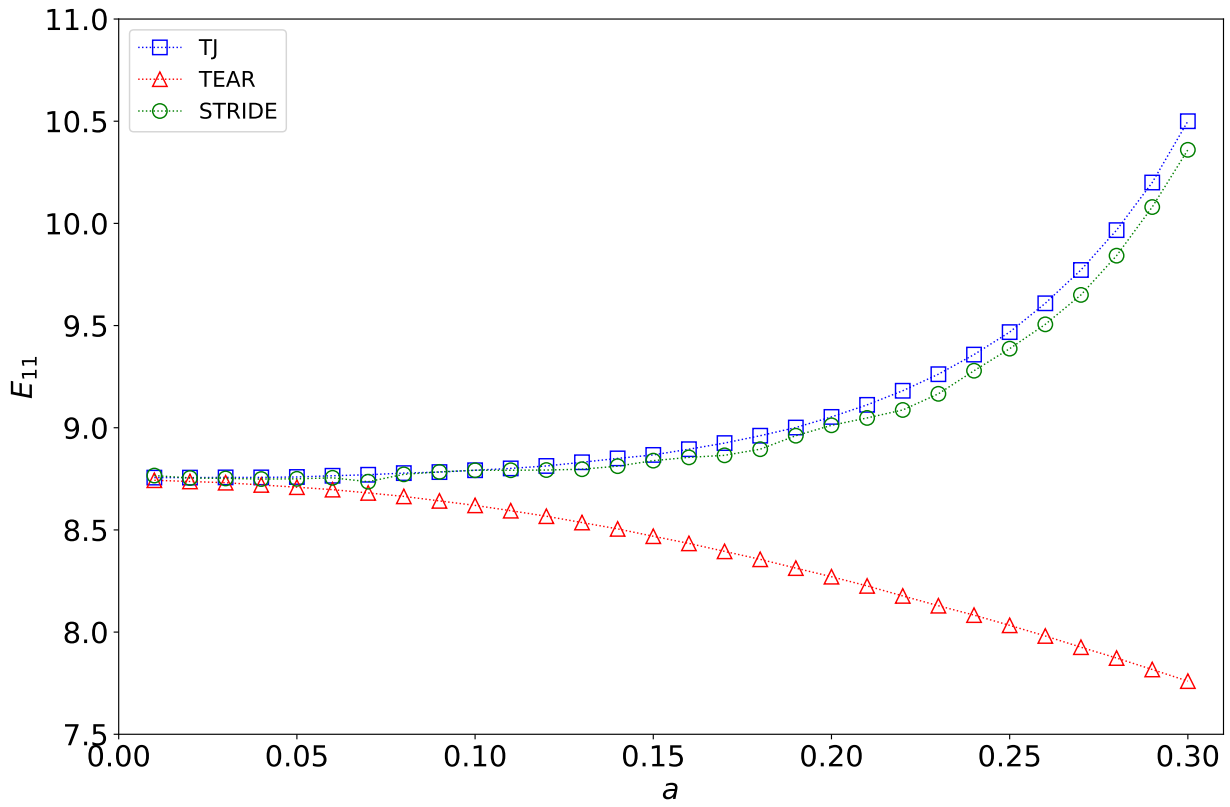

FIG. 1. TJ/STRIDE Benchmark Test 1. Circular cross-section: $q_0 = 1.1$, $p_\sigma = 1.36$, and $\beta_0 = 0.0$. Variation of the 2/1 tearing stability index with the inverse-aspect ratio, a.

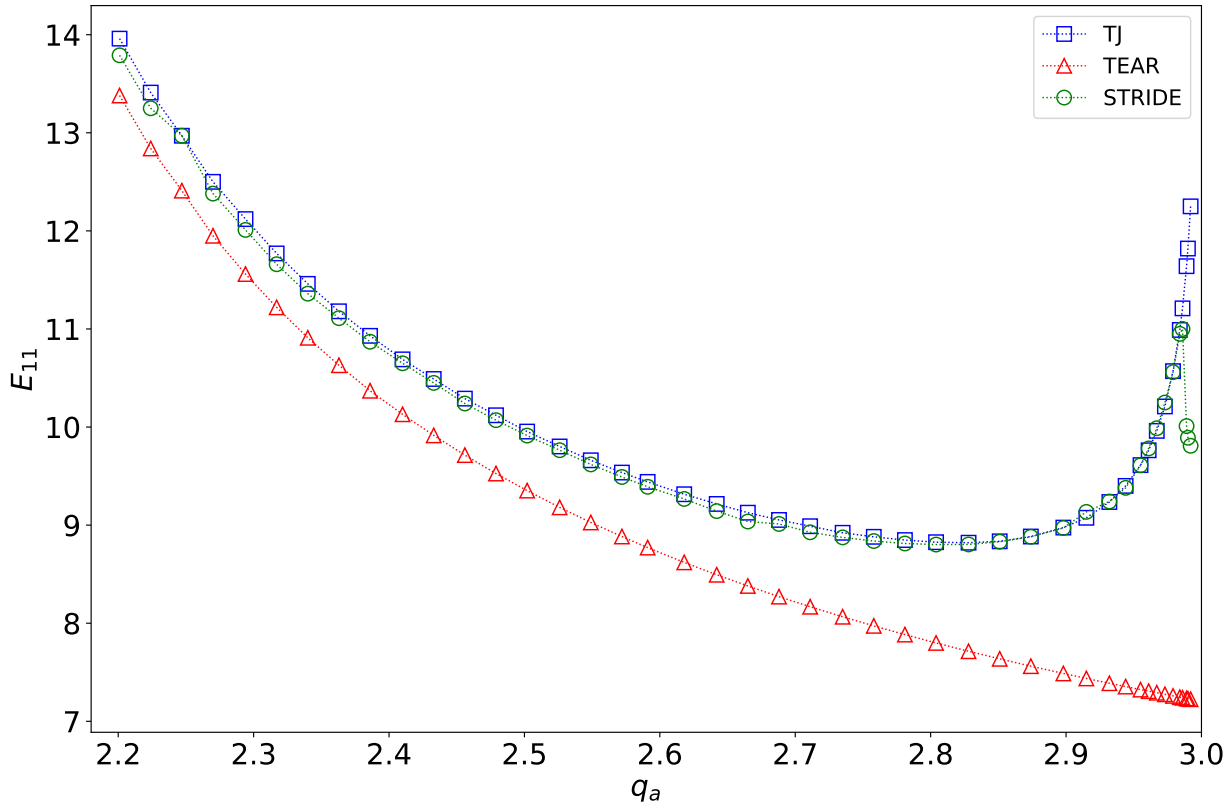

FIG. 2. TJ/STRIDE Benchmark Test 2. Circular cross-section: $q_0 = 1.1$, $a = 0.2$, and $\beta_0 = 0.0$. Variation of the 2/1 tearing stability index with the edge safety-factor, q_a.

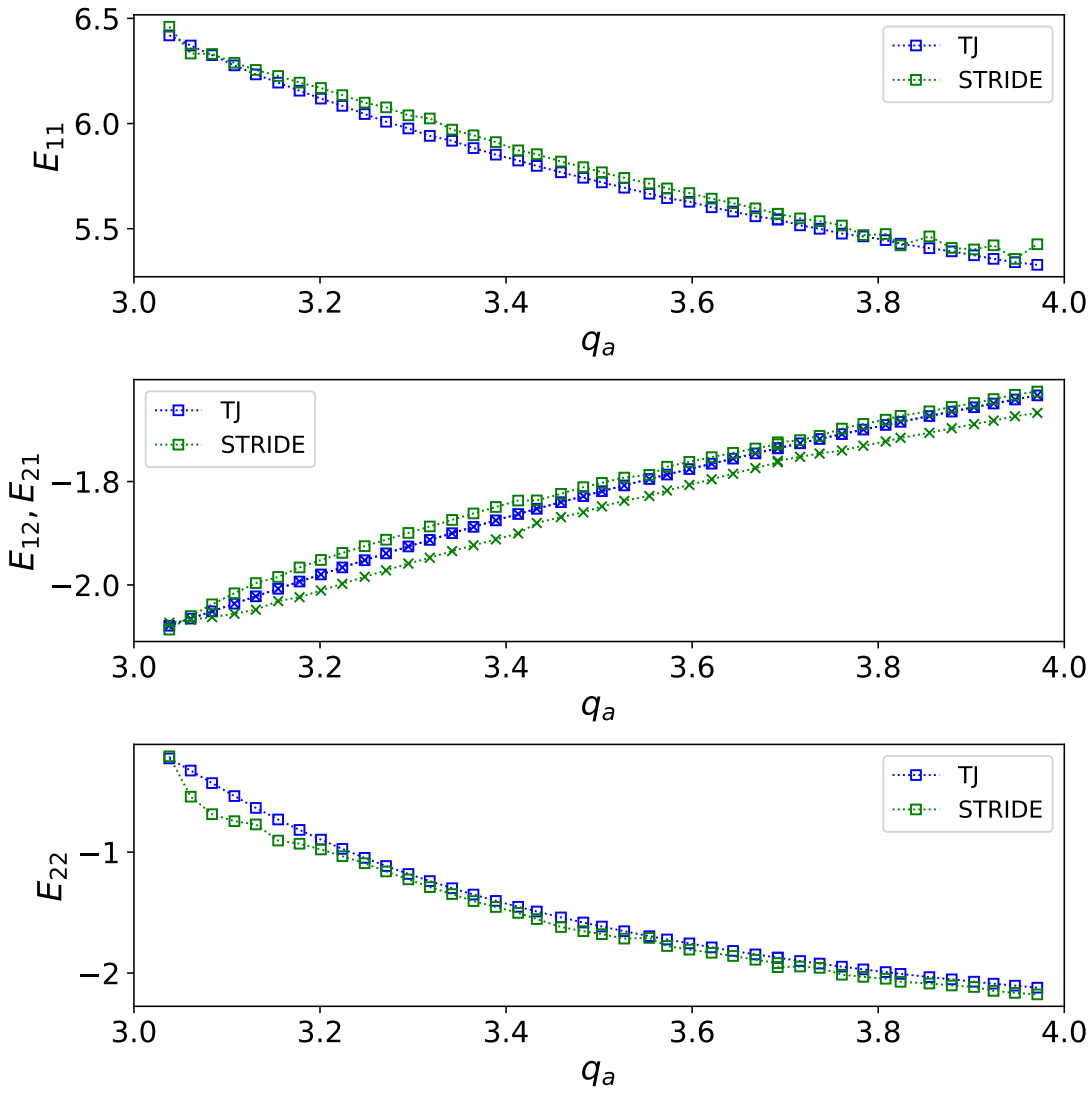

FIG. 3. TJ/STRIDE Benchmark Test 3. Circular cross-section: $q_0 = 1.1$, $a = 0.2$, and $\beta_0 = 0.0$. Variation of the elements of the tearing stability matrix with q_a. In the middle panel, the squares indicate E_{12} and the crosses indicate E_{21}.

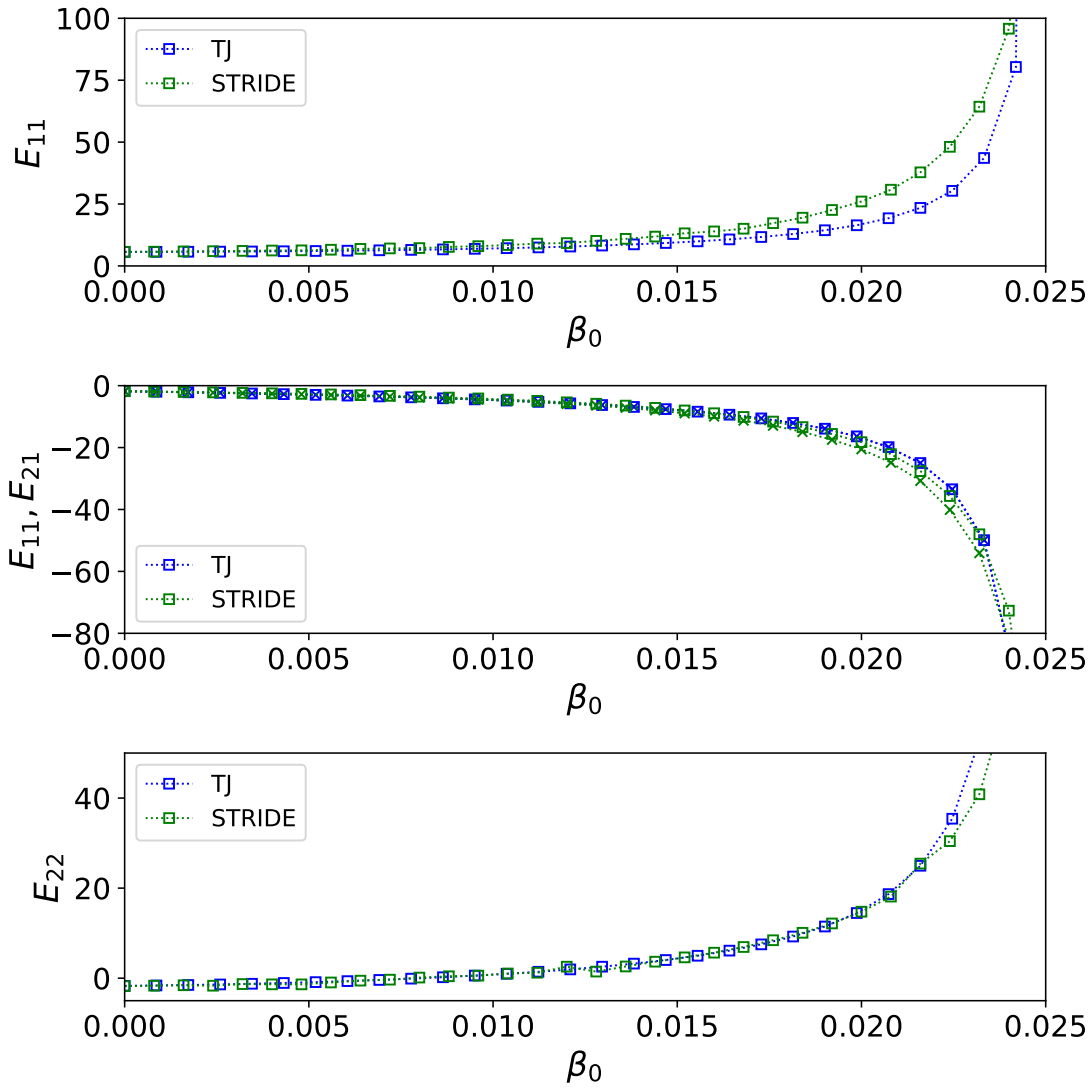

FIG. 4. TJ/STRIDE Benchmark Test 4. Circular cross-section: $q_0 = 1.1$, $a = 0.2$, $p_\sigma = 2.1$, and $p_p = 2.0$. Variation of the elements of the tearing stability matrix with the central plasma beta, β_0. In the middle panel, the squares indicate E_{12} and the crosses indicate E_{21}. The TJ β_0 has been rescaled by a factor 1.08.